Chemical Engineering Journal 398 (2020) 125440

Contents lists available at ScienceDirect

Chemical Engineering Journal

journal homepage: www.elsevier.com/locate/cej

Nanostructured porous graphene for efficient removal of emerging contaminants (pharmaceuticals) from water

Ahmed M.E. Khalil[a,b,*], Fayyaz A. Memon[a,*], Tanveer A. Tabish[a,c], Deborah Salmon[d], Shaowei Zhang[a], David Butler[a]

[a] College of Engineering, Mathematics and Physical Sciences, University of Exeter, Exeter, Devon EX4 4QF, UK
[b] Department of Chemical Engineering, Faculty of Engineering, Cairo University, Giza 12613, Egypt
[c] UCL Cancer Institute, University College London, Bloomsbury, London WC1E 6DD, UK
[d] College of Life and Environmental Sciences, University of Exeter, Exeter, Devon EX4 4QD, UK

HIGHLIGHTS

- Adsorption mechanisms of 6 emerging contaminants (ECs) on porous graphene (PG) were revealed.
- The heterogeneous adsorption was mainly described by Toth and Sips isotherm models.
- PG's treatment efficiency for ECs mixture was broadly robust in real samples studies.
- Decontaminating ECs trace concentrations reached > 99% at a low dose of PG.
- PG showed a promising recyclability potential for the 6 ECs (10% drop after 4 cycles).

GRAPHICAL ABSTRACT

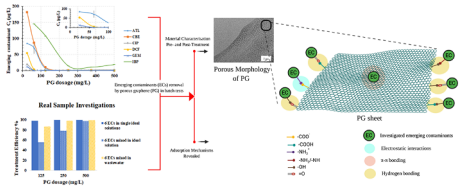

ARTICLE INFO

Keywords:
Emerging contaminants
Pharmaceuticals
Graphene-based materials
Porous graphene
Adsorption
Water and wastewater treatment

ABSTRACT

Pharmaceutical pollutants have become a worldwide concern. These emerging contaminants (ECs) are ubiquitously found in different water streams with concentrations above ecotoxicity endpoints, deteriorating aquatic life and water quality. This study evaluated extensively the efficacy of porous graphene (PG) synthesised at relatively low temperature as a potential candidate for the removal of six widely utilised pharmaceuticals from their aqueous solutions, such as atenolol (ATL), carbamazepine (CBZ), ciprofloxacin (CIP), diclofenac (DCF), gemfibrozil (GEM) and ibuprofen (IBP). Detailed batch tests were conducted to investigate the effects of adsorption time, initial EC concentration, PG dosage, solution pH, and temperature. Treatment efficiencies of ECs removal by PG were compared with those removed by carbonaceous counterparts (graphene oxide and graphite). Mixed solutions of these ECs were treated in different water bodies to test PG as a tertiary treatment option. The mechanism of adsorption was explored via thermodynamic studies, adsorption kinetics, and isotherm modelling, and characterisation of PG sorbent before and after ECs adsorption using TEM, SEM-EDS, XRD, FT-IR, Raman spectroscopy and other analyses. The results revealed fast kinetics and adsorption capacities exceeding 100 mg-EC/g-PG for some of ECs, and high removal efficiencies for trace concentrations of all selected ECs (> 99%) at a low dose of PG (100 mg/L). Removal efficiencies of mixed ECs in water and wastewater samples suffered from negative interferences, which can be mitigated by increasing the PG dosage. Adsorption processes were heterogeneous and controlled by physisorption. Further results showed the exothermic nature of the enthalpy-driven adsorption process and the recyclability potential of PG. It can be considered that PG could

* Corresponding authors at: College of Engineering, Mathematics and Physical Sciences, University of Exeter, Exeter, Devon EX4 4QF, UK (A.M.E. Khalil).
E-mail addresses: a.a.khalil@exeter.ac.uk (A.M.E. Khalil), f.a.memon@exeter.ac.uk (F.A. Memon).

https://doi.org/10.1016/j.cej.2020.125440
Received 12 March 2020; Received in revised form 8 May 2020; Accepted 10 May 2020
Available online 16 May 2020

be used as a promising candidate for efficient treatment of water contaminated with ECs related to the pharmaceutical group.

1. Introduction

Pharmaceuticals have emerged as potential emerging contaminants (ECs) over the last two decades. Their traces are rampant in ground and surface waters, typically at trace levels from ng/L to low μg/L, and even can be omnipresent in drinking waters [1,2]. Their existence in drinking water has raised great concerns regarding the long-term deleterious risks they might pose to human health and aquatic ecosystems [3]. Pharmaceuticals are originated from human and veterinary drugs and food additives and are generated into the environment initially via human or animal excreta with little or no change to their chemical structure [4]. Surface waters, groundwater and partially treated water contain pharmaceutical traces typically < 100 ng/l, while treated water has concentrations generally below 50 ng/l [5]. However, evidence on their detection and persistence in various natural freshwater resources is increasing worldwide. According to Fekadu et al. (2019), several pharmaceuticals were present in aquatic environments of both Africa and Europe in concentration levels higher than their ecotoxicity endpoints [6]. Pharmaceuticals are generally well characterised, and their impacts are assessed before commercialisation, so their negative effects are expected to result in the endocrine disruption in living organisms and development of antibiotic-resistant bacteria and genes [1,7].

Pharmaceuticals commonly found in water streams in India and the UK, such as atenolol (ATL), carbamazepine (CBZ), ciprofloxacin (CIP), diclofenac (DCF), gemfibrozil (GEM) and ibuprofen (IBP), were selected as model compounds for this study. ATL belongs to a class of pharmaceutical compounds known as beta-blockers, used to treat high blood pressure and heart rhythm disorders [8]. This class of drug is not effectively removed during wastewater treatment, characterised by long half-life (up to 166 days) and detected in various environmental water samples (varying from non-detected to 11 μg/L) [9]. Comparatively, CBZ is an antiepileptic drug that is most widely consumed to treat seizure disorders and relieve specific types of nerve pain such as trigeminal neuralgia [10]. It inhibits human embryonic cell growth [11] and bioaccumulates in freshwater and marine species, such as algae, bacteria, fish, and gastropods [12]. Among antibiotics, CIP is a highly used second-generation fluoroquinolone antibiotic [13]. The existence of this antibiotic in the environment can cause adverse effects to the microbial communities, leading to disturbances in the ecosystem [14]. DCF is a nonsteroidal anti-inflammatory drug (NSAID) used for pain and joint stiffness relief. However, it was reported that, with chronic human exposure, DCF may result in thyroid tumours and hemodynamic changes [15]. IBP is another widely used medication and is one of the top five most commonly consumed drugs in the UK [16]. IBP causes serious side effects to the human body including vomiting, bleeding, kidney problems, and cardiovascular risks [17,18]. Finally, GEM is a fibrates-type drug used to help lower fats (triglycerides) by reducing “bad” cholesterol (low-density lipoprotein) and raising “good” cholesterol (high-density lipoprotein) in the blood [19]. Like others, its presence in water might have environmental risks to humans, which are still unknown, and to marine organisms such as reducing testosterone levels in goldfish [20]. Numerous studies have proved that these contaminants are ubiquitously found in different aquatic environments and detected frequently in drinking waters with concentrations above ecotoxicity endpoints due to their poor metabolism and slow biodegradation [17,21-24]. Therefore, it is crucially important to design an appropriate technology that can cost-effectively achieve high removal rates and uptake capacities for these pharmaceuticals.

The wastewater and drinking-water treatment processes are not normally designed specifically to eliminate pharmaceuticals [5]. Therefore, strategies for the removal of pharmaceuticals from drinking water have been broadly explored. Advanced wastewater treatment processes (e.g., advanced oxidation, adsorption using activated carbon, ozonisation, nanofiltration membrane and reverse osmosis technologies) offer high removal rates (above 99%) for targeted pharmaceutical compounds [5,25]. Concerns are raised about the cost-effectiveness of these tertiary treatment processes. Most of them incur high costs and generate undesirable by-products. Of the above-mentioned techniques, adsorption seems to be a promising cost-effective technique for the removal of pharmaceuticals. It is simple to design and operate, has a low implementation cost compared to other technologies, offers high probability of recycling spent adsorbents and does not generate toxic by-products [26].

As far as adsorption and effective nano-adsorbents are concerned, graphene is an ideal nano-adsorbent for water treatment owing to its high theoretical specific surface area (SSA, 2630 m^2/g) and the presence of two basal planes of its single layer, available for contaminant adsorption [27]. In addition, the highly hydrophobic surface of graphene attracts organic contaminants with a strong adsorption affinity, such as chlorobenzenes, phenols, dyes and other toxic organic pollutants [28-30]. The removal of most under-investigated ECs (e.g., ATL, CBZ, CIP, DCF, and IBP) from water is mainly dominated by graphene oxide (GO) in literature [18,31-34]. GO has a nanosheet surface decorated with oxygen-containing functional groups (OCFGs) that results in a good hydrophilic characteristic and increased adsorptive affinity towards polar contaminants. However, in terms of higher surface area, superhydrophobicity, ease of separation from water, recyclability and chemical stability, porous graphene is a more attractive candidate for ECs removal, especially when it is produced by a low-cost scalable synthesis method [35,36]. In this regard, the reported technique used in this study for preparing PG structure was innovative as it only involved two steps after the preparation of GO, which did not involve the addition of a catalyst or use of any template [36]. Additionally, the temperature range involved was 190–200 °C, which was lower than that previously reported for the synthesis of porous reduced graphene oxide (rGO) [37]. In terms of application, up until now the treatment using graphene material has not been fully recognised for some of these contaminants (e.g., GEM). There have been only limited studies about the treatment of the considered ECs using graphene [38,39] in either single or mixed solution in different water matrices and the recyclability study was not provided.

The present work aims to test the adequacy and efficacy of a novel porous-type graphene material, synthesised at relatively low temperature, for ECs removal from water and uncover controlling mechanisms of the treatment. For that purpose, porous graphene (PG) with high SSA (679 m^2/g) was synthesised via a facile cost-effective route. The as-prepared PG and GO were used for the adsorption/removal of ATL, CBZ, CIP, DCF, IBP, and GEM drugs from aqueous media. All resemble different chemical structures and physicochemical properties in terms of hydrophobicity and hydrophilicity. The performance of the suggested graphene-based materials (GBMs) for the decontamination of six ECs was evaluated under different conditions of adsorbent dosages, single or mixed solution system, water bodies, contact time, pH and temperature. As-prepared and spent particles of PG were characterised by Fourier transform infrared (FT-IR), X-ray diffraction (XRD), Scanning electron microscopy – energy-dispersive X-ray spectroscopy (SEM-EDS), transmission electron microscopy (TEM), and Raman spectroscopy analyses for clarifying the sorption mechanisms. Furthermore, adsorption isotherms and kinetics of the nano-adsorbents

were studied using different thermodynamic and kinetic models and discussed to elucidate the adsorption behaviour. In addition, mechanisms and spontaneity of ECs adsorption were further illustrated by calculating the thermodynamic parameters. Finally, the recyclability of PG was addressed and assessed in several cycles for reliable application purposes.

2. Materials and methods

2.1. Chemicals, adsorbates and adsorbents preparation

Graphite (GI) powder (~20 μm), $NaNO_3$, H_2SO_4 (95.0–98.0%), $KMnO_4$, H_2O_2 (30 wt%), hydrazine (35 wt%), and analytical grades of pharmaceuticals, including ATL, CBZ, CIP, DCF sodium, GEM and IBP, were purchased from Sigma-Aldrich Co. (Poole, Dorset, UK), and formic acid (99.5 + %, LC-MS grade), sodium hydroxide and hydrochloric acid (36 wt%) were provided by Fisher Scientific Ltd. (Loughborough, UK). LC-MS grade acetonitrile and water were obtained from VWR international Ltd. (Lutterworth, UK).

PG was synthesised following the procedure reported previously by us [36], based on an inexpensive chemical oxidation – exfoliation – reduction – thermal treatment protocol. In brief, exfoliated graphene oxide flakes (around 1.5 nm in thickness, 0.5–20 μm in lateral size) were prepared following the modified Hummers' method. Initially, graphite flakes were oxidised by concentrated H_2SO_4, in the presence of $NaNO_3$, H_2O_2, and $KMnO_4$ as catalysts. The resultant graphite oxide was exfoliated and sonicated for 2 h in 500 mL suspension. 150 mL of GO solution was reduced by adding hydrazine (3 mL) in two stages (durations of 12 h and 2 h). The resultant rGO particles were vacuum filtered, washed with distilled water (200 mL) and thermally-treated by drying overnight at 200 °C under vacuum.

The pharmaceuticals were used to prepare standard stock solutions of ECs. All stock and standard solutions were prepared using distilled water (DW), unless stated otherwise. NaOH and HCl were used to adjust the pH of the prepared ECs solutions. All the solutions were surrounded by aluminium foil during storage and tests to prevent photo-degradation of the ECs. Suspensions of GI, GO and PG were sonicated for 10 min prior to their application in batch experiments.

2.2. Batch tests

Batch adsorption tests were carried out for each individual emerging contaminant under different conditions as illustrated below. All tests were repeated thrice, and the average values were taken for data analysis (Supplementary information, SI 1), which comprises kinetic modelling (SI 1.1), adsorption isotherm modelling (SI 1.2), and adsorption thermodynamics (SI 1.3).

2.2.1. Contact time

Kinetic studies were performed using EC initial concentration (C_0) of 10.5 mg/L (stock solution) for different contact-time intervals in separate experiments at room temperature (22 ± 3 °C) without pH adjustment ($pH_0 \approx 7.5$). 20 mL of pharmaceutical solution (ATL, CBZ, CIP, DCF, GEM or IBP) were placed in 60 mL bottles with screw caps. A certain amount of GI, GO or PG (5 mg from a suspension of 5-g adsorbent/L) was added into EC solution, followed by magnetic stirring/mixing for predetermined periods (t = 10, 20, 30, 50, 70, 90, 120, 240, or 300 min). The collected samples were filtered immediately through a 0.2 μm membrane filter.

2.2.2. Equilibrium experiment

Batch tests were carried out to evaluate the effects of variation in initial EC concentration (0.1–100 mg/L for ATL, CBZ, CIP, DCF, 0.1–15 mg/L for GEM, and 0.1–21 mg/L for IBP) using a fixed dosage of adsorbent (5 mg GI, GO or PG injected from a 5-g/L suspension). A mixture of pharmaceutical (20 mL) and graphite or GBM were shaken in 50 mL centrifuge tubes on a rotary shaker for 24 h. The supernatants of samples were acquired after vacuum filtration. Additionally, the effects of adsorbent dose variations of PG were explored by injecting specific amounts of 5-g/L PG suspension (0.1–2 mL) into a certain concentration of EC single solution, so that the initial concentration of EC after PG suspension addition was adjusted to 1 mg/L. Real sample investigations were carried out by applying the same specific amounts of 5-g/L PG suspension (0.1–2 mL) into ECs mixed solution spiked into distilled water (DW) or wastewater (WW) body. The initial concentration of each EC was set to 1 mg/L in either DW or WW. The domestic wastewater (partially treated) sample was collected from the final settlement tank of the secondary treatment unit prior to tertiary biological aerated flooded filter (BAFF) treatment unit, existing at Countess Wear Wastewater Treatment Works, South West Water Co., Exeter, Devon, UK. The characteristics of the WW sample are shown in Table S1. The collected WW sample was modified to contain ECs mixed solution and used immediately within one week after collection. If stored during that period, it was kept under 5 °C in a cold store.

2.2.3. Effect of pH and temperature

Batch adsorption tests were carried out for each EC under different pH and temperature conditions in 20 mL pharmaceutical solution of 10 mg/L with added PG (5 mg). In the cases of batch tests for the pH effect, the initial pH of EC solutions was adjusted to a specific value using (0.1 or 1 M) NaOH or HCl solutions and batch tests were conducted at room temperature (22 ± 3 °C). The pH of the solution after treatment was measured and found to be unchanged. The resulting suspensions of different pH values (2–11) were stirred on hotplate stirrers for 2 h at 200 rpm and the processed samples were separated via filtration using 0.2 μm membrane filter. To investigate the effect of temperature variation on adsorption, the pH of the solution was maintained at neutral level and tests were conducted at various temperatures (10–90 °C) under similar conditions described above (in 10 mg/L-EC solution of 20 mL volume treated with 5 mg-PG and stirred at 200 rpm for 2 h).

2.2.4. Reusability study

To evaluate the recyclability and reusability of PG, regeneration cycles were repeated four times. The conditions of the adsorption experiment were set at 5 mg PG dosage, 20 mL EC of 10 mg/L, 2 h contact time, 200 rpm stirring speed and room temperature. After sampling, the PG particles were allowed to settle, and the supernatant was withdrawn via a peristaltic pump. The spent particles were washed with DW and then subjected to a desorption process. NaOH solution (1 M) was applied as the desorption agent to recover ECs from the spent PG and the reaction mixture was stirred at 90 °C for 2 h. Subsequently, PG particles were rinsed twice with water and ethanol, and applied for a new cycle of adsorption. The regenerated nano-adsorbent was used for subsequent adsorption cycles under similar adsorption conditions to those in the case with the freshly prepared PG.

2.3. Analytical methods

2.3.1. Characterisation techniques

GBMs (pre-adsorption samples) and spent PG particles (as post-adsorption samples) were characterised by SEM-EDS, TEM, XRD, FT-IR, Raman spectroscopy, and surface characterisation analyser.

The morphologies of GI, GO and PG samples were examined using SEM-EDS (TESCAN VEGA3 SEM fitted with X-MAXN EDS detector) under high vacuum condition with accelerating voltage 20 kV. For GO, images were acquired from gold-coated samples and all the samples were mounted onto conductive carbon adhesive tapes.

High-resolution nanostructural images of as-prepared GO and PG were taken using a JEOL-2100 transmission electron microscope (TEM) operating at an accelerating voltage 200 kV. The powder sample was dispersed in ethanol and then dropped on the centre of a holy carbon-coated copper grid using a micropipette.

For FT-IR measurements, Infrared (IR) absorbance spectra were obtained between 500 and 2000 cm^{-1} at a resolution of 4 cm^{-1} using 20 co-added scans. 5 mg of material particles were thoroughly mixed with 180 mg of potassium bromide (KBr) in an agate mortar. Pellets were formed by pressing the resulting mixtures under 5 tons for 2 min. Each pellet was placed into an attachment and then analysed in the optical compartment of FT-IR (Bruker Optics Tensor-27) instrument.

Nanocrystalline composition of samples was determined by XRD analysis performed with an X-ray diffractometer from Bruker (D8 advanced). XRD patterns were recorded using Cu Kα radiation at 40 kV and 40 mA over 2θ range of 10-50° with a scan rate of 2° (2θ). Additionally, the Raman spectra were acquired using laser excitation of wavelength 532 nm operated at 6 mW power and emitted from Renishaw RM-1000 diode as a continuous wave.

The N_2 adsorption Brunauer-Emmett-Teller (BET) method was used to determine the SSA, porosity, pore volume and pore size of the PG. The nitrogen gas sorption analysis was carried out using a Quantachrome Autosorb-iQ gas area characterisation analyser. PG samples were heated to 200 °C under vacuum for 4 h to remove any contaminants inside pores prior to cooling in an external bath to −195.8 °C (77.2 K). Nitrogen gas was introduced to the evacuated sample chamber where the pressure and the total volume of gas were measured. The results from the gas sorption experiment are presented as a nitrogen adsorption–desorption isotherm curves in a graph, presenting the amount of gas adsorbed against the relative pressure in the chamber. For further inspection, the particle size and zeta potential were measured using Zetasizer Nano ZS (Malvern Panalytical Ltd, Malvern, UK) to further characterise PG and investigated ECs at the pH of the adsorption.

The wettability of GO, PG and ECs samples was examined using a contact angle goniometer. Images of each droplet were captured on a digital camera and analysed using the contact angle plugin in the software ImageJ. The contact angle value indicates the hydrophobicity of the material: hydrophobic in the case of $> 90°$ and hydrophilic in the case of $< 90°$ [40].

2.3.2. Measurement of ECs concentrations in solutions

A UV–vis absorption spectrophotometer was used to measure ATL, CBZ, CIP, DCF, GEM and IBP sample concentrations at 226, 285, 272, 275, 220 and 221 nm, respectively [18,38,41-44]. In addition, EC samples of lower concentrations (below 1 mg/L) were measured using Liquid Chromatograph (LC) equipped with a mass selective (MS) detector. Quantitative analysis of these six pharmaceutical drugs was performed using an Agilent 6420B triple quadrupole (QQQ) mass spectrometer (Agilent Technologies, Palo Alto, USA) hyphenated to a 1200 series Rapid Resolution HPLC system. 5 µl of the sample was loaded onto an Eclipse Plus C18 3.5 µm, 2.1 × 150 mm reverse-phase analytical column (Agilent Technologies, Palo Alto, USA). For detection using negative ion mode, mobile phase (A) comprising 100% LC-MS grade H_2O, with 0.1% formic acid and mobile phase (B) was 100% acetonitrile (LC-MS grade). The following gradient was used: 0 min – 20% B; 4 min – 90% B; 8 min – 100% B; 10 min – 100% B; 11 min – 20% B followed by 4 min re-equilibration time. The flow rate was 0.3 mL/min and the column temperature was set at 30 °C for the

Table 1
Target compounds and their structures, main *m/z* ions, fragmentor and collision energy voltages, average retention time and limits of quantification (LOQ) for LC-MS analysis.

Compound	Structure	Precursor *m/z*	ID Product *m/z*	Qualifier Product *m/z*	Fragmentor Voltage (kV)	Collision Energy Voltages (kV)	Average RT (min)	LOQ (µg/L)
Atenolol	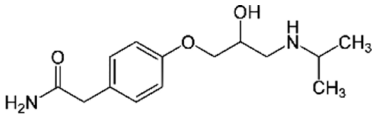	267.2	145.1	190.1	100	29 & 17	1.71	0.24
Carbamazepine	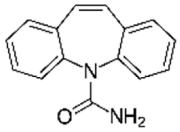	237.1	194.1	179.1	140	21 & 35	2.58	0.12
Ciprofloxacin	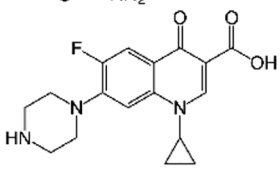	332.1	288.2	314.1	100	17 & 21	5.28	0.98
Diclofenac	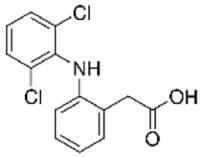	296.0	214.1	250.0	80	35 & 9	7.03	0.24
Gemfibrozil	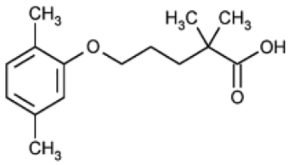	251.2	129.1	55.1	60	9 & 33	7.41	3.91
Ibuprofen	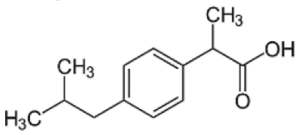	207.1	161.0	119.1	60	9 & 21	6.63	15.63

duration. The QQQ source conditions for electrospray ionisation were as follows: gas temperature 350 °C, drying gas flow rate of 11 L/min, nebuliser pressure 35 psig, and capillary voltage 4 kV. All ions were scanned in the negative ion mode and for a dwell time of 30 mseconds. The fragmentor voltage and collision energies had previously been optimised for each compound and are listed in Table 1, along with the compound retention times (RT) (in minutes), based on initial guidelines shown in previous reports [45,46]. Data analysis was undertaken using the Agilent Mass Hunter Quantitative analysis software for QQQ (version B.09.00). Concentrations were calculated from the standard concentration curves in the range of 1 mg/L to 0.06 μg/L, as were the limits of quantification (LOQs) for each compound (also in the table below). Four replicas were used for each test condition and the averages were compared.

3. Results and discussion

3.1. Adsorption batch studies

3.1.1. Effect of contact time and ECs adsorption kinetics

Batch tests were conducted for different contact times to acquire kinetic profiles for the six ECs adsorbed onto GI, GO and PG (Fig. 1). Fast sorption kinetics was observed in the initial stage of adsorption (60 min) for most of the ECs. Then the rate of adsorption decreased upon further increasing the time. The results indicated the outperformance of PG in overall, achieving removal efficiency of ECs above 40 to 60%. Hence, PG was found to be highly efficient for ECs removal in extremely low dosage (250 mg/L). The applied dosage is significantly low compared to that applied dosage for efficient pharmaceutical decontamination in other studies, involving treatment using

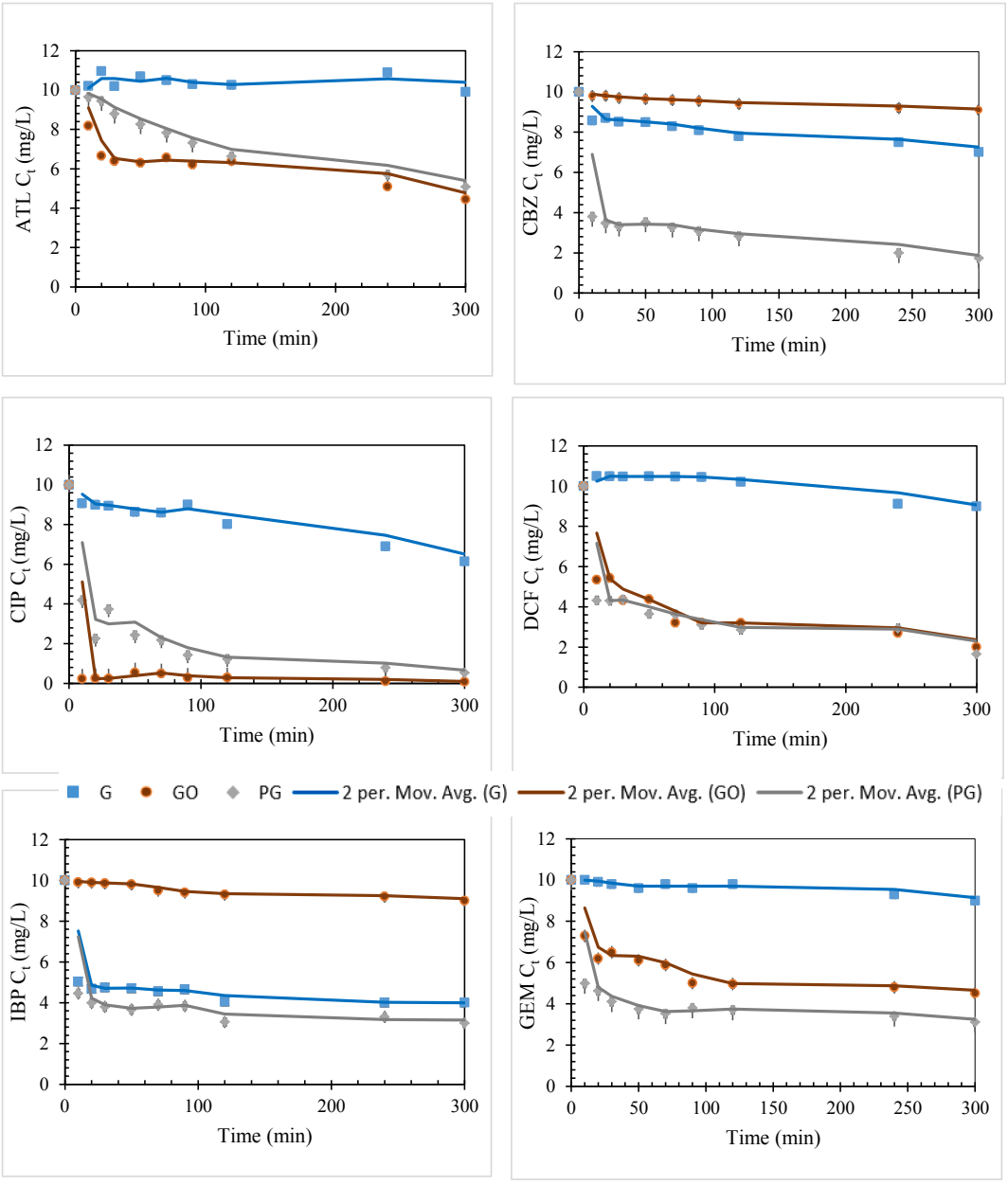

Fig. 1. Effect of contact time on adsorption of ATL, CBZ, CIP, DCF, IBP and GEM onto GI, GO and PG. Error bars were calculated based on standard deviation (Experimental conditions: number of runs 3; C_0 10 mg/L; adsorbent dosage 250 mg/L; pH 7.5; temperature 22 ± 3 °C). Graph dots and lines represent experimental results and their moving average fitting, respectively, and error bars indicate standard error of three replicates.

activated carbon (e.g., 3000 mg/L on average [2] and above 5000 mg/L [47]). To illustrate the sorption mechanism and the role of surface area and active sites, four kinetic models (SI 1.1) including pseudo-first order, pseudo-second order, Elovich and intraparticle diffusion reaction models were applied to evaluate the rate of adsorption reaction and its rate-controlling step. Of the four suggested models, the pseudo-second order rate model best described the kinetics of ECs adsorption onto GO and PG with an excellent fit as indicated by the highest correlation coefficient values (R^2 = 0.99 for most ECs). Table 2 lists the kinetic parameters and values of regression correlation coefficients (R^2) for each model. Kinetics of adsorption could be related to the hydrophilicity/hydrophobicity of EC, which is indicated by n-octanol/water partitioning coefficient (K_{OW}) [34]. According to the log value of n-octanol/water partition coefficient (Log K_{OW} values) for ECs shown in the surface wettability results (section SI 2.2), ATL and CIP are hydrophilic compounds with more OCFGs (e.g., carbonyl and hydroxyl groups). This facilitates faster access to the active sites and oxygen moieties on GO surface compared with adsorption on the superhydrophobic surface of PG. Therefore, values of kinetic constant of pseudo-second order model for ATL and CIP adsorption are two orders and one order of magnitude higher than that of PG, respectively. On the contrary, rapid adsorption kinetics rate was recorded for the rest of ECs onto PG due to their hydrophobic interactions as IBP and GEM are hydrophobic contaminants and CBZ is slightly hydrophilic/hydrophobic in nature. Such hydrophobic interactions/effects between hydrophobes and water cause hydrophobes (PG and EC of hydrophobic nature) to be attracted to each other and oriented away from water [48].

3.1.2. Effect of adsorbate initial concentration and ECs adsorption isotherms

Equilibrium studies were conducted to reveal the effect of initial EC concentration on the process of adsorption onto GI, GO and PG. Fig. 2 presents the isothermal data of ECs adsorption, revealing the relationship between equilibrium adsorption capacities of GI, GO and PG for ECs and concentrations of ECs in aqueous solutions at equilibrium. The isothermal experiments were carried out at room temperature (22 ± 3 °C) and with a mass of adsorbent of 5 mg (fixed dosage 250 mg/L). The results indicated further affinity of ECs of hydrophilic nature, such as ATL and CIP towards GO, while the other ECs were more attracted to PG and to a lower extent to GI. It should be noted that PG performance was not far poorer than that of GO, as indicated by the maximum adsorption capacities of GO and PG (calculated from batch test results) for ECs listed in Table S2. In general, although the adsorption performance of GO was higher for ATL and CIP removal, but, in terms of superhydrophobicity, ease of separation from water, recyclability and chemical stability, PG is a more attractive candidate for ECs removal in water treatment applications [36,49]. Thus, PG nanosheets outperformed their GBM counterparts. To elucidate further, seven adsorption isotherm models were evaluated for best fit to the experimental data. The calculated parameters of these models (Eqs. (S6-S12) in SI 1.2), including maximum adsorption capacities (q_s), are given in Table 3. In terms of the best match criterion (R^2), the Sips and Toth models are more appropriate for describing the adsorption equilibrium data for ECs onto GO and PG. Also, adsorption results of GO for ATL and CBZ could be depicted by the Freundlich model (Table 3), which agrees with that reported previously [31,34]. These results indicated heterogeneous adsorption arising from the distribution of surface sites which varied in abundance, type and strength for GO that resulted from the presence of OCFGs, planar surface and edge sites, and possible zones of different polarisability. However, PG adsorption performance for ATL, CIP, CBZ, DCF, and GEM and that of GO for ATL, CIP and GEM follows the Toth model. As stated earlier, the Freundlich and Toth isotherm models are plausible for describing heterogeneous multilayer adsorption. IBP adsorption data for GO and PG is represented by the Langmuir isotherm similar to what was reported in conducted studies on GO [18]. This seemed to suggest that, in the case of IBP adsorption onto a GBM surface, a monolayer coverage was formed, implying that the binding energy of each IBP molecule on the surface GO was uniform. Hence it is concluded that the GO molecules did not interact with one another during the IBP adsorption. Finally, in the case of DCF adsorbed by GO and PG, it was found that the Toth and Langmuir models fairly yielded a better fitting than the other models. In all cases, the value of the main energy of adsorption E (kJ/mol), which is related to the D-R model, can predict the type of adsorption. The observed low values of E parameter in Table 3 indicated that ECs adsorption process on GO and PG demonstrated physical characteristics [50].

3.1.3. Effect of adsorbent dosage on ECs removal in single and mixed solution

Fig. S1 illustrates the effect of PG dosage (25–500 mg/L) on the trace concentration of ECs, revealing that with increasing the dosage of PG, the concentrations of ECs dropped significantly (below 5 μg/L), especially after 100 mg/L of PG dose. Such improved removal performance is attributed to the availability of more active and accessible adsorption sites with higher dosages. In addition, PG can be considered a formidable remediator capable of treating these ECs even in real mixed solution (e.g. drinking water contaminated with ECs mixture) due to the low concentrations of ECs in actual drinking water and the high reactivity of PG nanosheets.

The applicability of PG to the removal of the selected pharmaceutical ECs was further investigated as a tertiary treatment option if used

Table 2
Values of fitted kinetic parameters for ECs adsorption by PG and GO (10 mg/L initial EC concentration, adsorbent dosage 250 mg/L, pH 7.5, temperature 22 ± 3 °C).

Experiment	Pseudo first-order parameters k_1		Pseudo second-order parameters			Elovich equation parameters b			Intra-particle diffusion equation Parameters C		
	(min^{-1})	R^2	q_e(mg/g)	k_2 (g/(mg.min))	R^2	a (mg/(g.min))	(g/mg)	R^2	k_p (mg/(g. $min^{1/2}$))	(mg/g)	R^2
ATL-PG	0.0089	0.995	36.55	0.00012	0.99	0.423	0.148	0.99	1.265	−1.224	0.976
ATL-GO	0.0099	0.772	16.12	0.01211	0.99	15.134	0.396	0.61	1.076	5.352	0.805
CIP-PG	0.0126	0.834	40.88	0.00205	0.99	157.088	0.233	0.84	1.733	15.740	0.644
CIP-GO	0.0144	0.434	41.78	0.01543	0.99	9.12E + 98	5.725	0.09	1.327	25.898	0.305
CBZ-PG	0.0104	0.779	35.31	0.00241	0.99	8174.061	0.418	0.83	1.351	15.421	0.559
CBZ-GO	0.0087	0.985	4.76	0.00212	0.91	0.125	1.115	0.91	0.217	−0.0178	0.991
IBP-PG	0.0111	0.405	29.44	0.00604	0.99	556522.223	0.636	0.78	1.088	15.036	0.462
IBP-GO	0.0073	0.912	7.96	0.00046	0.61	0.096	0.841	0.91	0.262	−0.396	0.928
DCF-PG	0.0057	0.517	30.62	0.00491	0.99	305.819	0.318	0.81	1.420	13.082	0.641
DCF-GO	0.0086	0.761	31.11	0.00321	0.99	31.141	0.235	0.94	1.520	11.021	0.743
GEM-PG	0.0095	0.566	28.98	0.00544	0.99	6595.591	0.475	0.89	1.128	13.881	0.516
GEM-GO	0.0269	0.892	22.96	0.00314	0.99	15.499	0.320	0.89	1.052	7.552	0.721

$0.9 \leq R^2 \leq 0.95$: underlined, $R^2 > 0.95$: bolded. R^2 is related to the accuracy of the fitted model. The values of R^2 were highlighted to draw attention to the best models.

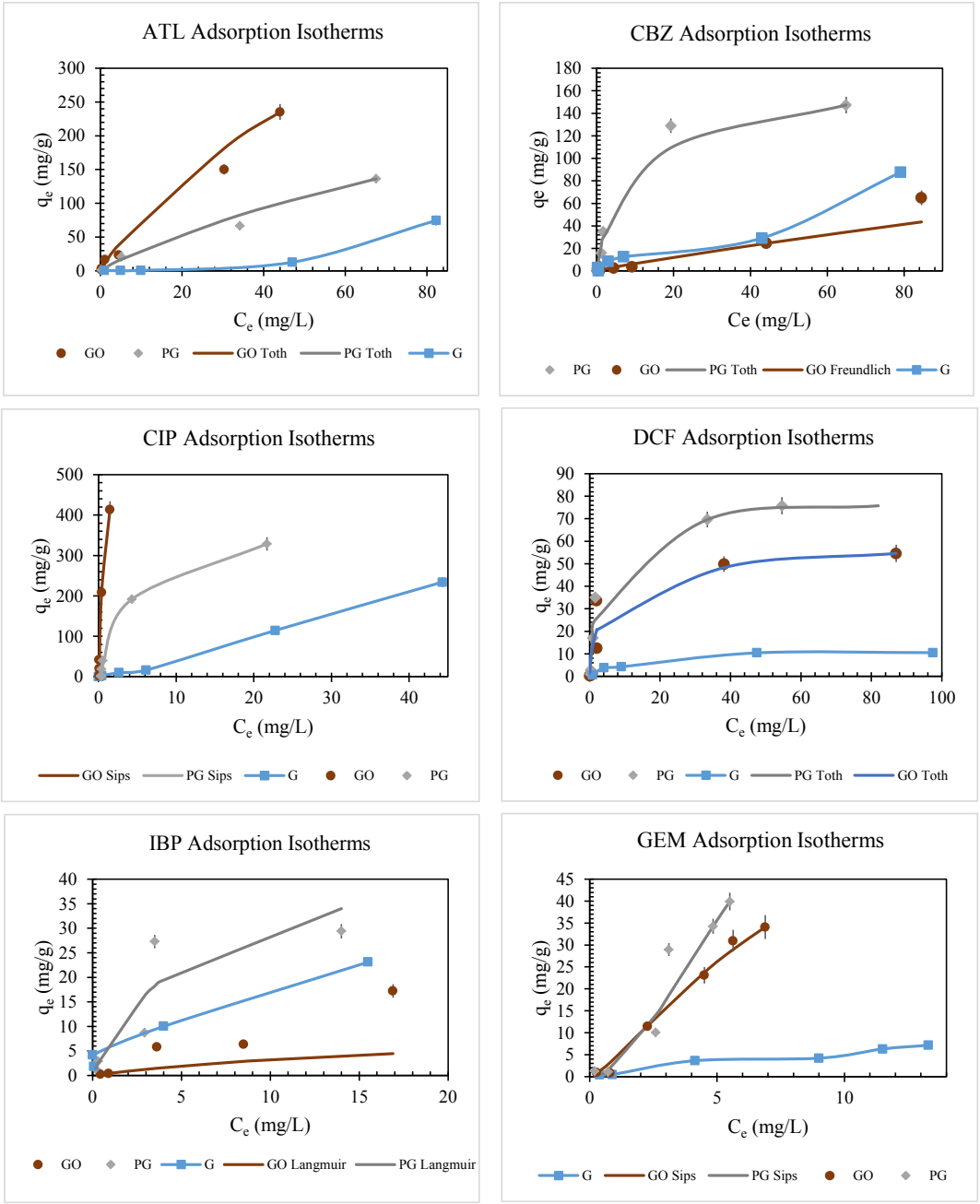

Fig. 2. Adsorption isotherms of six investigated ECs onto G, GO and PG. Solid lines represent suggested model simulation. Experimental conditions: 250 mg/L adsorbent, pH 7.5, temperature 22 ± 3 °C. Error bars indicate standard error of three replicates.

as an adsorbent in treating ECs mixtures in DW and WW matrices. Initially, the concentration of pharmaceuticals in the collected WW sample could not be detected by LC-MS analysis (below detection limit). Afterward, two water bodies (DW and WW) were spiked with the selected ECs to obtain final concentrations of 1 mg/L for each EC. These mixtures could be considered as real environmental aqueous samples, especially WW samples. Then PG was applied to these samples with various dosages (25–500 mg/L) and its treatment/concentration profiles are shown in Fig. 3. In general, the presence of all ECs in one medium (DW or WW) affected the removal of each EC by PG, so the concentrations of treated mixed solution samples were higher than that of treated EC (single) solution samples. This should be attributed to the competition between these drugs to occupy the active adsorption sites of PG, which resulted in a general negative interference effect. Such effect was often observed in numerous studies that dealt with real sample investigations [33,39,51-55]. A significant increase in EC concentration appeared in mixed ECs solution of DW matrix after treatment apart from CIP for which the removal performance of PG was not drastically degraded. According to Table S2 and Table 3, CIP has the highest affinity among other selected ECs towards PG with maximum adsorption capacity of ca. 370 mg-CIP/g-PG (Sips model, $R^2 = 1$). Such affinity of CIP is shown clearly in Fig. 3 where the negative interference effect on PG removal performance for CIP in mixed solution compared to that for CIP in single solution (both in DW body) was minimum. On the contrary, the treatment of IBP in mixed solution samples has shown the highest final concentrations, lowest treatment efficiencies and strongest negative interference, due to the lowest maximum IBP adsorption capacity (compared to that of other ECs) of PG of ca. 48 mg/g (Table 3, Langmuir isotherm, $R^2 = 0.98$). One way to improve the treatment efficiencies of ECs mixed in DW samples is to increase the

Table 3
Equilibrium parameters for the adsorption of ATL, CIP, CBZ, IBP, DCF and GEM onto PG and GO. Experimental conditions: 250 mg/L adsorbent, pH 7.5, temperature 22 ± 3 °C.

Experiment	Freundlich model Parameters			Langmuir model Parameters			Tempkin model Parameters			D-R model Parameters		
	k_F (mg/g)	n_f	R^2	q_s (mg/g)	k_L (L/mg)	R^2	B_1	k_T (L/g)	R^2	q_s (mg/g)	E (kJ/mol)	R^2
ATL-PG	2.738	1.071	**0.961**	8.87	0.445	0.712	21.445	1.75	0.8	33.66	1.38	0.60
ATL-GO	7.598	1.303	0.946	117.13	0.076	0.867	15.001	3.61	0.88	38.36	1.69	0.91
CIP-PG	18.5091	0.878	0.697	−7.33	−0.554	0.351	77.066	3.101	**1**	342.63	1.10	0.88
CIP-GO	281.77	0.677	0.564	25.62	2.183	0.025	145.711	10.592	**0.95**	309.71	2.24	0.49
CBZ-PG	12.2785	1.446	0.919	14.63	2.611	0.721	23.618	5.376	0.87	40.17	2.80	0.54
CBZ-GO	0.864	1.132	**0.968**	8.89	0.138	**0.992**	9.611	0.897	0.64	9.77	1.20	0.55
IBP-PG	6.267	1.339	0.901	47.85	0.175	**0.982**	7.006	5.801	0.76	21.14	1.95	0.87
IBP-GO	0.563	0.822	**0.952**	10.01	0.044	**0.978**	3.699	1.448	0.73	6.95	1.02	0.82
DCF-PG	7.671	1.564	0.761	91.59	0.103	**0.963**	13.433	4.526	**0.98**	58.06	1.38	**0.98**
DCF-GO	3.658	1.139	0.796	2.43	3.064	0.831	7.869	7.387	0.74	8.97	2.91	0.48
GEM-PG	4.604	0.842	0.865	9.26	0.663	0.530	11.533	2.993	0.75	17.98	1.78	0.55
GEM-GO	2.981	0.781	0.901	9.48	0.342	0.542	10.701	2.3044	0.86	16.88	1.47	0.61

Experiment	Elovich model Parameters			Toth model Parameters				Sips model Parameters			
	q_s (mg/g)	k_E (g/mg)	R^2	q_s (mg/g)	n	K_T (mg/g)	R^2	K_S (L/mg)	q_s (mg/g)	z	R^2
ATL-PG	385.31	0.007	0.1	1455.36	0.51	0.050	**0.984**	0.457	71.81	0.916	0.7
ATL-GO	64.73	0.161	0.6	1656.02	0.58	0.053	**0.981**	0.029	282.8	6.661	**0.99**
CIP-PG	−115.64	−0.110	0.2	409.15	0.94	0.246	**0.995**	0.246	370.11	1.239	**1**
CIP-GO	−79.58	−0.718	0.4	624.10	1.10	1.151	**0.970**	2.515	417.79	3.541	**0.99**
CBZ-PG	88.96	0.210	0.6	191.67	0.72	0.242	**0.984**	0.204	154.251	1.188	**1**
CBZ-GO	2092.89	0.00034	0	139.80	0.54	0.178	0.841	0.175	27.491	1.067	0.59
DCF-PG	41.23	0.295	0.4	82.74	0.79	0.433	**0.974**	0.559	75.801	1.970	**1**
DCF-GO	−17.52	−0.147	0.6	65.95	0.51	1.031	0.836	0.083	68.646	0.845	0.79
IBP-PG	71.17	0.096	0.1	110.30	0.20	2.037	0.758	0.139	49.508	0.572	0.76
IBP-GO	−20.53	−0.027	0.4	72.87	0.16	1.477	0.794	0.097	18.791	4.869	0.89
GEM-PG	−38.73	−0.081	0.5	160.86	0.815	0.118	0.902	0.134	109.710	1.810	0.92
GEM-GO	−33.11	−0.067	0.5	574.72	0.80	0.025	**0.999**	0.120	78.257	1.345	**0.99**

$0.9 \leq R^2 \leq 0.95$: underlined, $R^2 > 0.95$: bolded. R^2 is related to the accuracy of the fitted model. The values of R^2 were highlighted to draw attention to the best models.

dose of PG around 5 times. 100 mg/L of PG was sufficient to treat concentrations of ECs (1 mg/L) single solutions with removal efficiencies above 99%. From Fig. 3, raising the dosage of PG to 500 mg/L improves the removal efficiencies of ATL, CBZ, CIP, DCF, GEM and IBP to 99.6%, 99.2%, 99.9%, 99.8%, 99.7% and 88.2%, respectively.

Similarly, treated samples of ECs mixed and spiked into WW body suffered an increase in EC concentration if compared to the concentration of treated EC single aqueous solution (Fig. 3). The modified wastewater samples contained mixed ECs and were rich in ammonia and chlorides (as indicated in Table S1), which could influence the adsorption process by PG. Nevertheless, on the contrary, Fig. 3 indicates that treated real environmental samples of WW have shown lower concentrations compared with treated mixed ECs of DW for most of the ECs. It should be noted that the withdrawn WW samples were collected from the final settling tank of the secondary treatment unit just before BAFF treatment, which involves a sort of biological remediation. Therefore, the WW sample enclosed microbial content and these targeted ECs are mainly organic compounds and could still be removed to various degrees by any bacterial action. For instance, biological treatment has various removal rates for pharmaceuticals ranging from < 20% to > 90% depending on several factors including sludge age, activated sludge tank temperature and hydraulic retention time [5]. In spite of the fact that GBMs have developed a demonstrated antibacterial activity [56], it might be difficult to eliminate the whole microbial content given that the PG dose was significantly low, and different competing organic contaminants, ammonium ions , chloride ions and other ions were present to interfere with PG bactericidal activity. As being an antibiotic, CIP could resist that bacterial action and its concentrations in the treated WW samples were relatively higher than CIP concentrations in single or mixed solution of DW background. In addition, the effect of the ionic strength on the adsorption of CIP onto graphene and graphene oxide was explored and the presence of chloride ions caused a decline in their adsorption capacity [33,39]. It was suggested that the possible reasons for such lower performance were attributed to the electrostatic screening of concentrated cation ions (Ca^{2+}, Na^+ accompanying chlorides) and the salting-out effect that could reduce the solubility of CIP in water and encourage hydrophobic partitioning of CIP to graphene.

Regarding the treatment performance of PG in pharmaceuticals contaminated wastewater samples, the reduction in removal efficiency is generally lower than that in DW samples containing mixed contaminants. This observation indicates that the performance of PG would be refined and improved by utilising an excess dosage of PG lower than that used for mixed ECs solution of DW samples. From the graphs in Fig. 3, applying around 2.5 times the dose of PG suggested for single EC in DW matrix (equivalent to 250 mg/L) would be sufficient to reduce ECs concentrations significantly (below 15 μg/L).

3.1.4. Effect of pH on adsorption of ECs onto PG

The effect of pH on ECs adsorption onto PG was investigated, and ECs concentration profiles are shown in Fig. 4. When pH < 8, there was no significant change in the final concentration of ECs (after 2 h), while increasing pH above 9 favoured desorption of the contaminants. This may be owing to the electrostatic repulsion between the negatively charged ECs ions and the PG nano-sheet covered with negative hydroxide ions. This hypothesis was confirmed via testing the zeta potential of PG, which varies from −20 to −45 mV by increasing the pH of PG suspension as reported by us [36]. A previous study investigated IBP removal by GO nanoplatelets (GONPs) has shown the increase in the treatment efficiency by increasing the pH value, while the removal efficiency was drastically reduced at higher pH values (> 8) [18]. Additionally, adsorption of the beta-blocker ATL on GO was reported to have an identical reaction to the pH change similar to the one given in this study by PG [31]. The highest pharmaceutical removal was

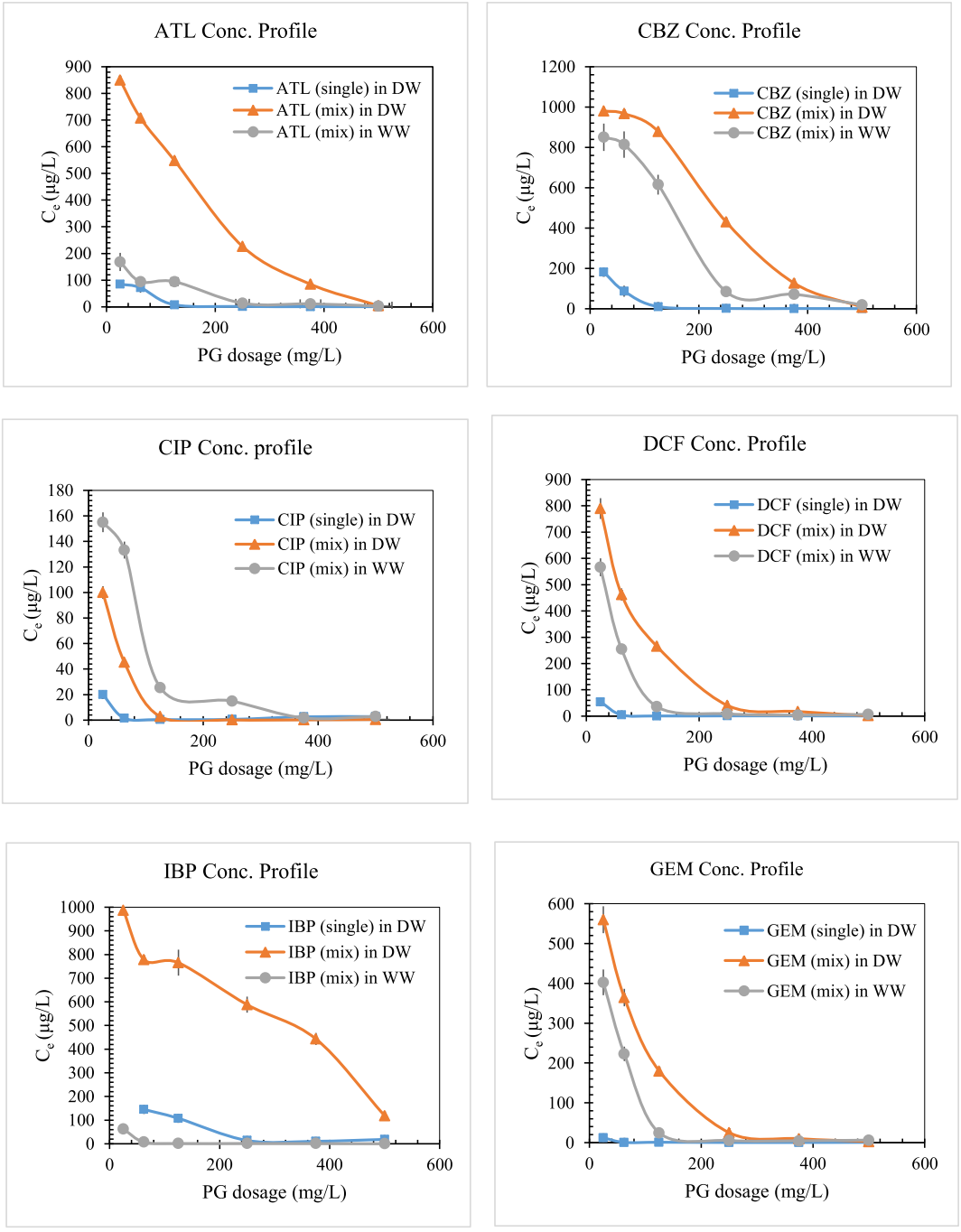

Fig. 3. Effect of adsorbent dosage on the removal of EC in distilled water and wastewater bodies (single or mixed solution, contact time: 24 h; pH (DW) 7.5; pH (WW) 7.1; initial individual EC concentration in single or mixed solution: 1 mg/L). Error bars indicate standard error of four replicates.

achieved at strong acidic conditions (pH 2). When the pH value increased from 2 to slightly acidic condition (pH 5) and then to an alkaline condition (pH 8), the removal of ATL decreased. This desorption behaviour can be used to plan a route for regenerating spent PG nanosheets to reuse them several times in water treatment.

3.1.5. *Temperature variation effect and thermodynamic modelling*

The effect of solution temperature on the behaviour of ECs adsorption onto PG was studied (Fig. 5). Generally, raising the solution temperature led to significant increases in contaminant concentrations and decreases in adsorption of pharmaceutical pollutants from their solutions by PG. Thermodynamic parameters of EC adsorption behaviour were estimated according to equations discussed in SI 1.3. By plotting ln D vs. 1/T (Eq. (S16)) for the adsorption of ECs by PG, straight lines were obtained (Fig. S2), with correlation coefficients given in Table 4. The calculated thermodynamic parameters (in Table 4) reveal more information about the nature of the adsorption process between ECs and PG and determine the feasibility and spontaneity of the adsorption process. The negative values of ΔH confirm the exothermic nature of the adsorption, which explains the decrease in adsorption at higher temperatures. The magnitude of ΔH suggests a weak type of bonding between ECs by PG, such as physical adsorption (ΔH range between −20 to −40 kJ/mol), rather than chemical adsorption (ΔH range between −400 and −80 kJ/mol) [57]. The negative values of ΔS, suggest a decrease in randomness attributed to the decrease in the degree of freedom of pharmaceutical molecules. The

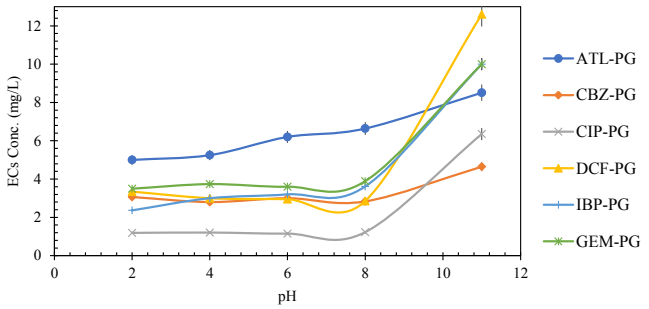

Fig. 4. Effect of pH on ECs adsorption onto PG (Experimental conditions: 5 mg PG dosage, 20 mL EC of 10 mg/L, 2h contact time, 200 rpm stirring speed, room temperature). Error bars indicate standard error of three replicates.

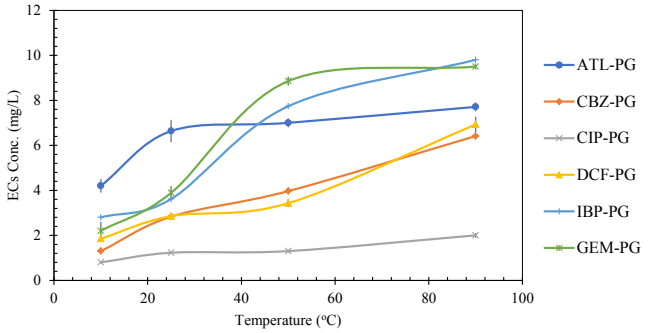

Fig. 5. Effect of temperature on ECs adsorption onto PG (Experimental conditions: 5 mg PG dosage, 20 mL EC of 10 mg/L, 2 h contact time, 200 rpm stirring speed). Error bars indicate standard error of three replicates.

free energy change, ΔG, is negative, for a product-favoured and spontaneous reaction and an indication of an enthalpy-driven process.

The results of the thermodynamic analysis presented in this study are in agreement with previous studies that investigated the sorption of different pharmaceutical pollutants onto graphene and graphene oxide nanoplatelets [18,51]. For instance, aspirin, acetaminophen, and caffeine adsorption by graphene nanoplatelets (GNPs) and IBP removal by GONPs were tested at different temperatures [18,51]. The feasibility and spontaneity of both adsorption processes were described by thermodynamic analysis. In both aforementioned reports, the rise in temperature led to a decline in the sorption process, indicating a physisorption process which was exothermic in its nature.

3.1.6. Recyclability of PG

Recyclability experiment was carried out to demonstrate the reusability of PG. The conditions were assigned according to the previous investigations on the effect of pH and temperature variations. The PG particles were recycled four times after regeneration via heating at 90 °C in a basic solution of 1 M NaOH and then washing repeatedly with water and ethanol. The shown graph in Fig. 6 illustrates the recyclability of PG in the ECs uptake process. The graphene material showed reasonable EC removal capabilities with recycling for a number of cycles without any major loss in sorption. In these cycles, the removal efficiency suffered a little decrease, which was most likely due to an incomplete regeneration process and adsorbent mass loss. Mainly, the

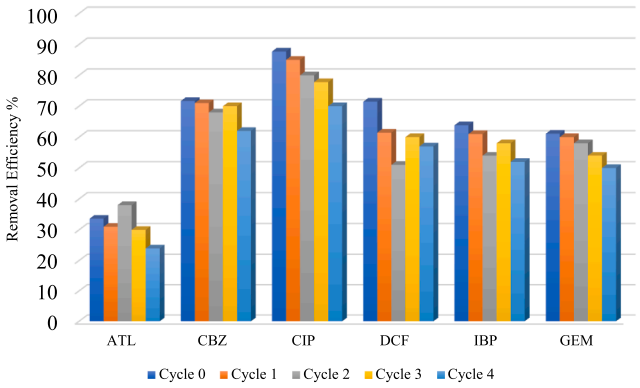

Fig. 6. Recyclability of PG for the adsorption of ECs (Experimental conditions of adsorption test: 5 mg PG dosage, 20 mL EC of 10 mg/L, 2 h contact time, 200 rpm stirring speed).

loss in adsorbent quantity was due to unsettled nanoparticles, which occurred during the repeated settling processes of PG. Therefore, the loss in ECs removal efficiency after four consecutive adsorption-desorption cycles was about 10% drop in its absolute value as seen from Fig. 6.

A limited number of studies investigated the desorption characteristics and recyclability of GBMs, adsorbing these ECs from their aqueous solutions [18,34]. Graphene oxide nanoplatelets (GONPs) were reused for 10 cycles to remove IBP from water and regenerated by treating with 4.0 M HNO_3 [18]. The rate of IBP removal by GONPs attained values above 95%. In a different report, partial CBZ recovery (about 26%) from graphene oxide occurred by repeated washings with water for eight desorption cycles [34]. It was assumed that chemisorption could occur and covalent bonds might be formed between the functional groups on the organic chemical CBZ (amide group) and OCFGs on GO. However, the reusability of GO was possible by desorbing CBZ with ethanol, resulting in a CBZ recovery of about 93% detected in three cycles. This observation showed the physisorption process of CBZ adsorption onto GO. Similarly, the physisorption of the six targeted ECs onto PG was detected and revealed in this study by different analytical methods, such as analysis of adsorption isotherm models and thermodynamic analysis of temperature variation.

According to our previous report, PG has proved superior regeneration, cycling efficiency (over 90% as treatment efficiency after 5 cycles) and suitability for the decontamination of several target contaminants [36]. In fact, the capacity of PG for oil adsorption could last with treatment efficiencies above 90% even after 15 cycles. Arsenic, dyes (methylene blue and rhodamine B), fluoride and nitrate were subsequently adsorbed by PG and recovered. The adsorption capacities of PG for inorganic and organic contaminants were slightly affected after 5 cycles, losing 10% of the total treatment efficiency. In this study, the same behaviour was observed with ECs related to the organic group. These results emphasise on the experimentally-proved recyclability of the PG material. Optimisation strategies could be implemented in future works to investigate the optimum conditions for PG regeneration for more cost-effective recycling. For instance, preliminary recyclability tests showed the effect of temperature rise (from 50 °C to 90 °C) was not

Table 4
Thermodynamic parameters for the adsorption of ECs onto PG.

Parameters	ATL	CBZ	CIP	DCF	IBP	GEM
R^2 of ln *D* vs. *1/T* plot	0.793	0.968	0.922	0.944	0.972	0.939
Δ*H* (kJ/mole)	−14.371	−25.000	−10.190	−23.380	−53.470	−47.590
Δ*S* (kJ/mole.K)	−0.039	−0.061	−0.004	−0.057	−0.165	−0.146
Δ*G* (kJ/mole)	−2.861	−6.471	−8.840	−6.131	−4.051	−3.951

significantly high on ECs desorption from PG. In addition, the amount of washing liquid contributed considerably in PG regeneration.

3.2. Material characterisation and adsorption mechanism

Material characterisation was performed pre- and post-EC treatment to elicit more insights into adsorption properties of sorbents and the sorption mechanism. Surface morphology and composition of the investigated materials were discussed as below, while their specific surface area, particle size, surface charge, and surface wettability were shown in SI 2 (Further investigation on properties of GBMs and ECs).

3.2.1. Surface morphology

The surface features of GI, as-prepared GO and PG were examined using SEM and are shown in Fig. 7 and Fig. S3. Raw material GI particles exhibited flaky texture (Fig. 7A and Fig. S3(a, b)). After the oxidation of these GI flakes and consequent exfoliation of their resultant particles, GO was prepared, showing a noticeable sheet-like layered structure (Fig. 7B and Fig. S3(c, d). The material developed in this study (PG) has a nanostructural morphology, which has evidently been supported by pore size using surface characterisation analyser (4 nm as average pore size, Table S4 in SI 2.1). However, partial agglomeration and stacking was observed in GBMs, especially between PG nanosheets. Due to their small cross sectional sizes and high specific surface area (Table S4), PG nanosheets were more prone to aggregation and clustering (Fig. 7C and Fig. S3(e, f)). Wrinkles, defects and corrugations are visualised in GO and PG nanosheets in SEM images, which are revealed more clearly by high-resolution TEM images (Figs. S4 and S5). The structure of PG was revealed as a transparent irregular, folded nanosheets interweaved with each other. The formation of nano-sized channels or pores $<$ 5 nm on PG surface was confirmed (Fig. 7D).

The composition of adsorbents was detected prior to adsorption experiments using energy dispersive X-ray spectroscopy attached to SEM and TEM instruments. Results are given in Figs. S6 and S7 and Table S3. Graphite was almost 99% carbon with some traces of oxygen, while GO had a higher oxygen content, attesting the presence of OCFGs and a carbon-to-oxygen ratio of 2.6 on average. PG had a majority of carbon content, but still some OCFGs were available in its composition to a certain extent. Regarding the composition of elements in the spent particle of PG post adsorption with ECs, Table S3 lists the elemental composition (%) of carbon, nitrogen, oxygen, fluorine and chlorine. The obtained results agreed with the elements found in the structural formula of pharmaceutical compounds in Table 1. According to Table S3, C, O and N were presented in ATL-PG and CBZ-PG spent; C, N, O and F or Cl were detected in CIP-PG and DCF-PG spent, respectively; and GEM-PG and IBP-PG contained C and O only. This detection proved the occurrence of adsorption process on the sheet surface of PG and made these samples reliable for further investigations using XRD, FT-IR and Raman spectroscopy for more insights into the adsorption mechanism.

3.2.2. Surface composition

Material properties of PG were inspected before and after adsorption of ECs to elucidate the adsorption mechanism. Prior to adsorption experiments, adsorbents were characterised using X-ray diffraction and FT-IR spectroscopy and their patterns are presented together in Fig. S8. Each adsorbent exhibited its characteristic peaks at 26° (2θ) for GI, 12.6° for GO and 24.4° for PG [36]. In comparison to these XRD patterns, it is observed the broadening of (0 0 2) lattice peak for PG and reduction of its intensity compared to that of graphite, and this is an indication of graphene sheet formation. After adsorption of EC by PG, there was no significant change in the patterns shown in Fig. S9. Identical diffraction patterns were developed, indicating no

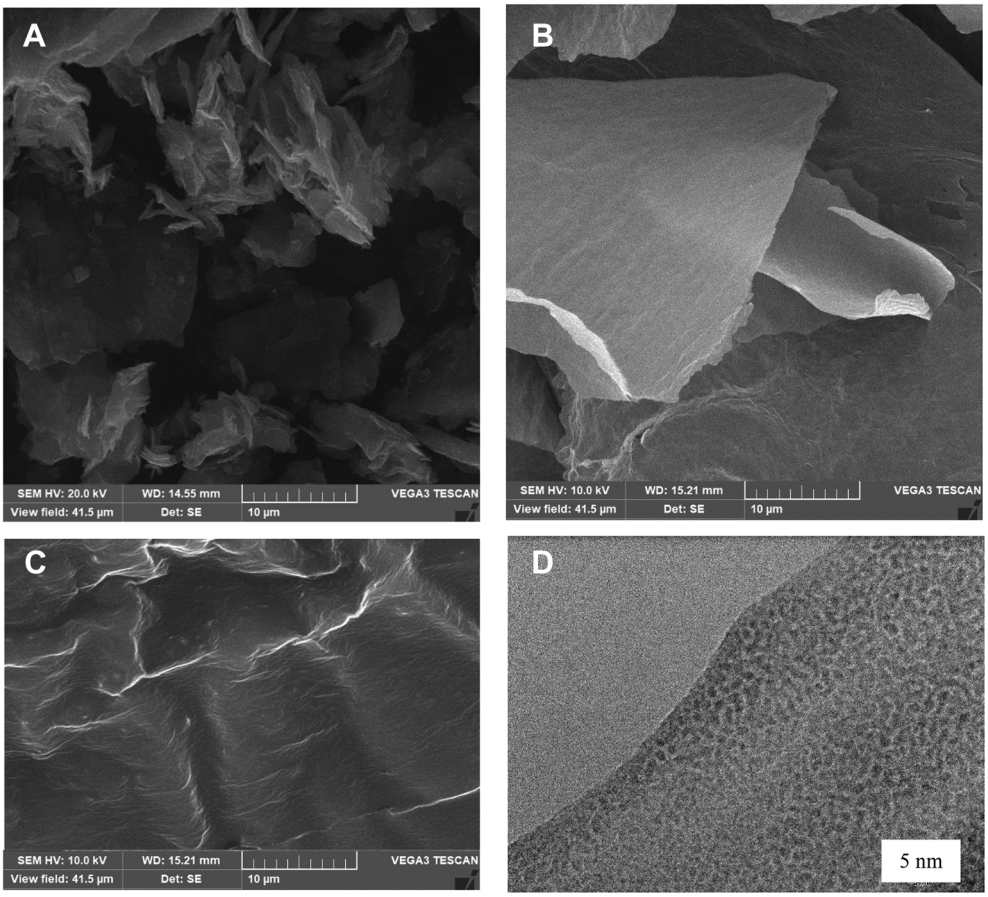

Fig. 7. SEM Images of (A) GI, (B) GO and (C) PG. (D) High-resolution TEM image of PG showing porous morphology.

considerable alteration in crystal structure and composition. Regarding FT-IR patterns, Fig. S8b presents characteristic bands of distinguishable functional groups; 1052, 1246, 1384 cm^{-1} (C–O stretching in epoxy group),1627, 1678, 1732 cm^{-1} (C═C stretching in aromatic ring), 2362 cm^{-1} (C═O stretching in carboxylic acid), 2849, 2922 cm^{-1} (C–H stretching vibrations) and 3444 cm^{-1} (O–H stretching vibrations) [31,39]. Graphs presented in Fig. 8 include the FT-IR spectra of ECs, which have a strong peak at 3356 cm^{-1} (for ATL) ascribed to N–H skeletal vibrations of both primary and secondary amine (–NH_2 and –NH), and a medium peak at 3172 cm^{-1} owing to hydrogen bonding of O–H stretching and at 3434 cm^{-1} corresponding to free O–H stretching vibrations [31]. Moreover, C═O, C═C and C–O–H stretching vibrations were found at several positions, e.g., at 1638 cm^{-1}, 1582 cm^{-1} and 1417 cm^{-1}, respectively. The FT-IR spectra of PG before and after EC adsorption revealed that although most of the peaks of EC were not observable after EC adsorption, the peaks corresponding to the stretching vibration of C═C bonds shifted from 1630 to 1633, 1637, 1634 cm^{-1} after ATL, CBZ and CIP adsorption, respectively, and to 1638, 1637, 1636 cm^{-1} after DCF, GEM and IBP adsorption, respectively. In agreement with previous findings in different reports [36,38,39], the peak shift, in this case, portrays the role of π-π interaction between EC and PG in the adsorption process. Other small shifts were recorded elsewhere around peak regions, identifying O–H stretching vibrations for ATL, GEM and IBP adsorption, showing that

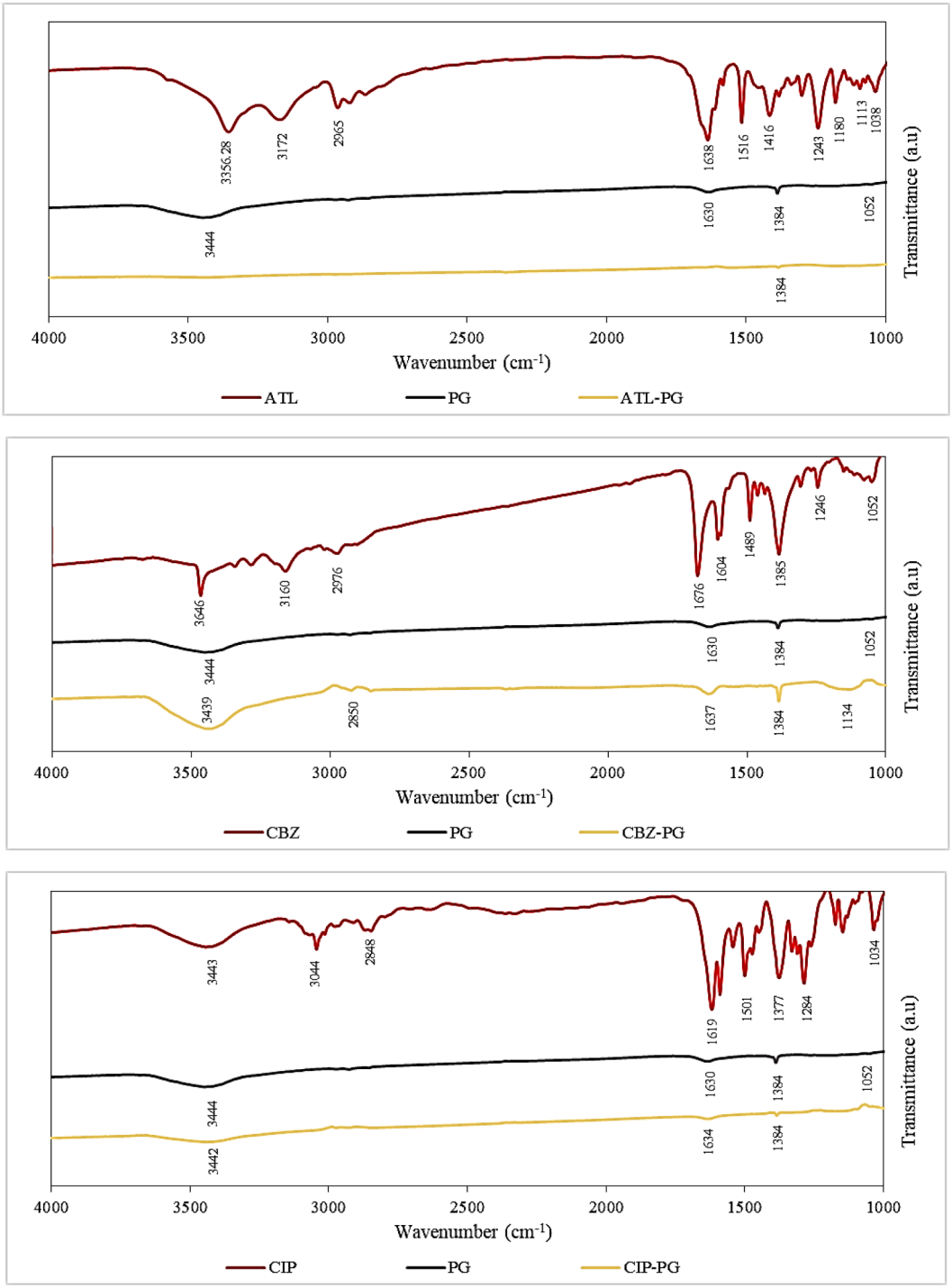

Fig. 8. FT-IR spectra of PG before and after adsorption of the pharmaceutical contaminants (Adsorption conditions: 10 mg/L solution, 250 mg/L PG dose).

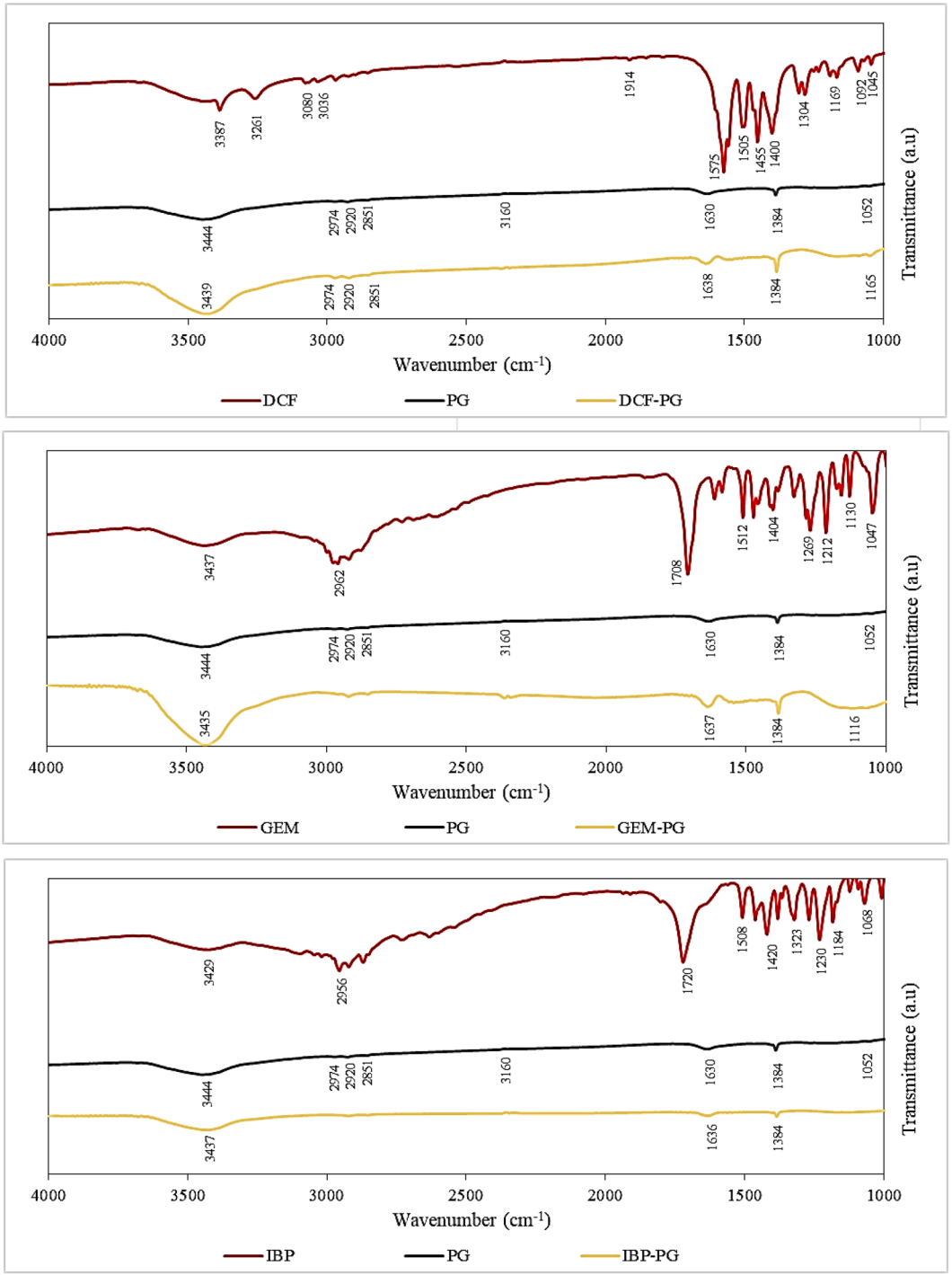

Fig. 8. (*continued*)

PG interacted with some ECs via a few hydrogen bonds. In general, some peaks of FT-IR spectrum of PG after adsorption were clearly shifted, indicating that the functional groups of PG were still remained. However, ascribed to physisorption, the bands appeared weakened and broadened after adsorption in Fig. 8.

On the other hand, Raman spectroscopy was conducted for the qualitative analysis of graphene before and after adsorption of ECs (Figs. S11 and S12). Peaks of Raman patterns for PG are not shown clearly in Fig. S12 due to the high intensity of bands exhibited by all ECs. The plots of Raman spectra of ECs of our particular interest depicted their features, representing distinct bond types and the availability of different bonding sites for possible interactions with adsorbents. In Fig. S11, a more illustrative Raman pattern for PG showed peaks of G and D bands [58]. The band shape of 2D was distorted which caused its broadening, giving a particular evidence for Bernal stacking of layers that is witnessed in exfoliated graphene. The Raman G-peak was detected at ca. 1577 cm^{-1} and was indicative of the sp^2-hybridized hexagonal lattice of carbon atoms, while the D-peak was located at ca. 1330 cm^{-1}, which corresponds to sp^3-hybridized hexagonal lattice of carbon atoms that represented the defects on the edges of the graphene [59,60]. The ID/IG ratio of as-prepared pristine PG was almost equal to unity, providing that the activation of nanosheets for the formation of pores and edges in the PG layers occurred ascribed to the increased amount of sp^3-hybrdized carbon atoms. Small shifts in G

and D bands and generation of new bands at around 558, 785, 950 and 1088 cm^{-1} were found in Raman spectra of spent PG post adsorption of ECs (Figs. S11 and S12). These new patterns resembled the intercalation of EC molecules in the inter-layer space of PG. In addition, the existence of new bands in the region of relatively lower frequency vibrations suggested the formation of weak bonds might be as a result of π-π interactions, hydrogen bonding and van der Waals (vdW) forces.

3.2.3. Adsorption mechanism

Based on the aforementioned analyses and discussions, this section summarises the findings extracted from characterisation of materials pre- and post-adsorption, adsorption isotherm and thermodynamic studies. The following dominant adsorption mechanisms were deduced at several points of this study from the low absolute values of ΔH in thermodynamic studies, from low values of main energy of adsorption in D-R model, and from analysing spent PG using FT-IR analysis and Raman spectroscopy. Firstly, PG had several types of OCFGs, such as (such as carboxylic (–COOH), hydroxyl (–OH), and epoxy (–C–O–C–)) and active sites arising from the abundance of porous architected channels on its large surface area. Taking that into account, the affinity in the adsorption process between PG and contaminants having different sizes relied on the high surface area, porous structure and availability of significant transformation sites. Secondly, the surface charge and protonation-deprotonation transition of functional groups on the active sites of the PG surface under different pH conditions play a crucial role in the adsorption process. Pharmaceutical with both primary amine ($–NH_2$) group, such as ATL and CBZ, and secondary amine (–NH) group, such as CIP and DCF, can react with PG as indicated by equations below:

$$PG - COO^- + Drug - NH_3^+ \xrightarrow{\text{Electrostatic forces}} PG - COO^-NH_3^+ - Drug \quad (1)$$

$$PG - OH + Drug - NH_2 \xrightarrow{\text{Hydrogen bonding}} PG - OH\cdots NH_2 - Drug \quad (2)$$

$$PG - OH + Drug - NH \xrightarrow{\text{Hydrogen bonding}} PG - \overset{H}{O}\cdots\overset{H}{HN} - Drug \quad (3)$$

$$PG - OH + Drug - NH \xrightarrow{\text{Hydrogenbonding}} PG - OH\cdots NH - Drug \quad (4)$$

$$PG - OH + Drug - NH \xrightarrow{\text{Hydrogen bonding}} PG - \overset{H}{O}\cdots HN - Drug \quad (5)$$

Electrostatic interactions could occur between mainly the protonated amine groups $- NH_3^+$ and between the negatively charged groups of PG (e.g., $–COO^-$) as in Eq. (1). Additionally, surface-bridging via H-bonding could possibly exist between the hydrogen atoms of hydroxyl groups of PG and nitrogen atoms of amine groups of drug molecules (Eqs. (2) and (4)) or the oxygen atoms of hydroxyl groups of PG and hydrogen atoms of amine groups of drug molecules (Eqs. (3) and (5)). Also, hydrogen bonding could take place between all of pharmaceuticals and PG as follows (Eqs. (6) and (7)):

$$PG - COOH + Drug = O \xrightarrow{\text{Hydrogen bonding}} PG - COOH\cdots O = Drug \quad (6)$$

$$PG - OH + Drug = O \xrightarrow{\text{Hydrogen bonding}} PG - OH\cdots O = Drug \quad (7)$$

Moreover, hydrophobic effects and π–π interactions between the localized π electrons in the conjugated aromatic rings of the PG and the pharmaceutical molecules could contribute to the adsorption mechanism.

Other weaker interactions such as van der Waals forces could exist as well. And all these suggested interactions are in a reasonable agreement with similar effects and interactions previously reported for the adsorption of different ECs on GO materials [18,28,31,32,34].

It becomes obvious how drugs such as CBZ and CIP can be readily adsorbed by PG (Fig. 1 and Table S2). For instance, the presence of three aromatic rings, primary amine group and carbonyl group in CBZ structure (Table 1) offered more than three types of interactions. Especially under acidic conditions (pH < pKa, acidity constant pKa of CBZ = 13.9), drug molecules existed in positively charged form due to the ease of NH_2 protonation. Comparatively, PG exhibited a negative charge state for the particles at all tested pH conditions as stated previously. Therefore, electrostatic and π–π interactions along with hydrogen bonding, and van der Waals (vdW) forces are all presented in the adsorption mechanism, resulting in high uptake by PG and fast kinetics. The hydrophobic nature of the drug also plays a vital role in adsorption via hydrophobic effects developed between drug molecules, PG sheets and water.

Carbonaceous compounds (PG, GO and GI) exhibit nearly the same aforementioned adsorption behaviour/mechanism towards the targeted contaminants, so electrostatic interactions, hydrogen bonding, π-π interaction and van der Waals (vdW) forces, all could exist in the adsorption mechanism but with a varying degree. This degree depends on the number of OCFGs on the adsorbent surface (high in the case of GO or very low for GI). Therefore, electrostatic and π-π interactions could dominantly occur between hydrophobic organic groups/molecules of the pollutants and carbon sheets of PG.

3.3. Water treatment potential of PG as a nano-adsorbent

Through the included investigations of this study, PG has proved its reliability for ECs removal from water and wastewater. Besides, PG could have higher adsorption capacities for conventional and emerging contaminants if applied in treatment works compared to ligand-based composite materials available in the literature [61]. According to our previous report, PG has shown its efficacy in eliminating arsenic, fluoride, nitrate, methylene blue, rhodamine B and oil from water [36]. For instance, the adsorption capacity of PG for arsenic exceeded 325 mg/g more than the reported values (82.40 mg/g or 142.25 mg/g) for some ligand-functionalized nano-conjugate materials [61,62]. The determined adsorption capacities of our suggested material (PG) in single adsorption experiments were 325, 375, 500, 313 and 375 mg/g-PG for arsenic, fluoride, nitrate, methylene blue, and rhodamine B, respectively [36]. Besides, PG has great values of pharmaceutical adsorption capacity often greater than those of other reported carbonaceous counterparts according to Table S2. Comparing these results with those in previous reports, Banerjee et al. prepared GONPs and investigated them for the adsorption of IBP from its aqueous solution, achieving a maximum adsorption capacity of only around 3.24 mg/g [18], while Kyzas et al. removed the beta-blocker ATL by GO with a maximum adsorption capacity of 116 mg/g [31]. GO was utilised to remove DCF and CIP with maximum adsorption capacities of 43.9 mg/g [32] and 379 mg/g [33]. Carboxyl-functionalised multi-walled carbon nanotubes (MWCNTs) and GAC possessed an adsorption capacity for CBZ of around 120 and 50 mg/g-sorbent, respectively [34]. Concerning graphene, Zhu et al. sorbed CIP onto graphene with a maximum adsorption capacity of 323 mg/g-G [39]. This value is close to that estimated in this current study for the maximum achieved adsorption

(8)

capacity of PG for CIP in experiments (329 mg/g, Table S2) and slightly lower than that maximum adsorption capacity calculated according to Sips isotherm model (370 mg/g, R^2 = 1, Table 3). GAC was tested in the same study for CIP removal with a maximum adsorption capacity of 217.4 mg/g-GAC [39]. The maximum adsorption capacity for the adsorption of DCF by rGO was reported as 59.67 mg/g [38]. From Table S2 and Table 3, the maximum recorded adsorption capacities of PG for DCF in experiments is 76 mg/g and, according to Langmuir, Toth and Sips adsorption models, are ca. 91.6 (R^2 = 0.963), 82.74 (R^2 = 0.974) and 75.8 (R^2 = 1), respectively. rGO had a much lower specific surface area (98 m^2/g) compared to that of suggested PG (ca. 670 m^2/g), which justifies the outperformance of PG in this study. Direct literature might not be available for the rest of the selected ECs removed by graphene.

Despite the extensive research into the graphene development for a variety of applications, the safety and environmental toxicity of graphene have been an issue for the safe and sustainable translation of graphene into an array of industrial markets. Our research group (Prof. Zhang) has extensively studied the toxicity, toxicokinetics, underlying toxicology mechanisms and influencing factors of graphene nanostructures towards the environment and living systems at cellular and molecular levels [63], such as PG foam [59], GO [64], rGO [65], PG [66] and graphene quantum dots [67]. Additionally, they have also studied the release of any toxic ions, free radicals, or unpaired electrons from graphene structures towards living systems in a dose- and concentration-dependent manner. These studies provide key insights into the transportation and uptake of PG architectures into the aquatic environment causing minimal levels of toxicity over 7 days of interaction of graphene with fish (as an aquatic animal model). It was concluded that porous architectures of graphene did not impose any potential threat to the aquatic organism, food uptake, and eventually to human health. Although long-term toxicity of graphene has not been explored yet. However, in water treatment systems, the use of graphene is time-specific which implies that limited concentration and dosage patterns of graphene are likely to be safe for aquatic organisms. Collectively, our group has illustrated that via tuning the physio-chemical features and surface properties of graphene nanostructures, environmental and biological safety of graphene can be improved in a dose- and time-dependent manner. While at low doses (such as 10 mg/ml concentration), graphene has been found less toxic and compatible with living systems [63,66]. In the current study, concentrations of 250 mg/L (on average) were used which are unlikely to have any noticeable toxic effects towards human and animal cells, organs, and tissues. These findings can potentially allow for the application of these graphene nanostructures in the environmental industry, including water and wastewater treatment.

The interaction of graphene with living systems in wastewater treatment applications is likely to be non-invasive in general. Such non-invasive interactions relatively induce less toxicity in comparison to other administration routes of graphene (intravenous) in the living systems for disease management (such as drug/gene delivery and light-mediated theranostic applications) [68]. While in water and wastewater treatment modalities, graphene-based absorbents are being used in treatment plants as an 'indirect' interaction with living systems. After the purification of water (and wastewater) with graphene, it is significantly important to evaluate whether treated water contains any graphene-related toxic ions. Potential risks resulting from the release of any toxic ions from graphene need to be evaluated. In the current work, using a wide range of analytical tools, PG structures were investigated before and after adsorption, revealing that graphene did not release any toxic ions. Additionally, the reuse, regeneration, and recyclability of graphene were investigated which also showed that graphene mass was not reduced up to toxic levels. Acute, sub-chronic, and chronic levels of toxicity are associated with invasive use (delivery, and implantation) and administration routes of graphene. Using such administration routes, the notions of biotransformation, bioaccumulation, biomagnification, biodistribution, and biosafety of graphene can be investigated by evaluating the toxicity levels in biological fluids and organs (such as heart, kidney, lungs, liver). These organs reveal the clearance and biodistribution of graphene in animal and human models [68,69]. As discussed earlier in this section, our group has recently investigated the biosafety of graphene nanostructures at cellular, tissue, and organ levels, revealing that the toxicity of graphene is dose-, time- and administration route dependent [59,63-67]. Taken together, the production route reported in this work enables the sustainable development of PG into water treatment applications. In addition, further research work is needed to fully elucidate the ecotoxicity of these materials associated with water treatment plants. These future studies may support the regulatory decision making and risk assessment for the successful realisation of PG-based materials into environmental applications.

Economically, PG is a cost-effective and environmentally friendly material of proved recyclability [36,49,70]. The facile production route stated for this superhydrophobic PG (based on heat treatment of rGO) was to unlock the current main bottlenecks in its commercial application. This thermal treatment process involved temperature range 190–200 °C, which was lower than that previously reported for the porous rGO synthesis (800 °C) [37]. More developments are possible for further improvements. For instance, the synthesis process mentioned in this study could be altered to follow a green approach based on iron-based graphene oxide synthesis and coconut oil reduction [70,71]. The produced rGO could be further thermally-treated at relatively low temperature as a key feature (discussed in this study and our previous study [36]) to produce highly porous graphene of higher specific surface area. This modified process is non-toxic, ultrafast (< 1 h preparation), safe and cheap (without sonication and with ease of separating the final product). Furthermore, PG nanosheet could be utilised as a reliable supporting material for various nanoparticles via cross-linkers to form novel evolutionary nanocomposites that act as a platform for environmental applications [49,72,73].

The removal technologies in tertiary treatment units are mainly responsible for eliminating ECs and, in particular, pharmaceutical contaminants. However, various studies have shown that the most common tertiary treatment technologies, such as granular activated carbon (GAC) and ozone treatment, could not eliminate efficiently resisting pharmaceutical compounds [25]. CBZ and GEM were among this list that resists treatment because of their physicochemical properties such as high water solubility and/or poor degradability [74]. In this study, PG showed high adsorption capacities for CBZ (154.25 mg/g, Sips model, R^2 = 1, Table 3) and GEM (40 mg/g, Table S2), fast kinetics (Fig. 1) and reliable performance in treating these contaminants in water and actual wastewater bodies spiked with single or mixed ECs solution (Fig. 3). Another issue is related to the treatment using activated carbons. They have been investigated as efficient adsorbents for the removal of pharmaceutical and personal care products (PPCPs), such as p-Chloro-m-xylenol [75], diclofenac, ibuprofen, ketoprofen, and naproxen [2,76] and triclosan [77]. However, regeneration of activated carbons (ACs) after adsorption is difficult, making the adsorption using ACs costly, not reliable and not applicable to large-scale treatment processes [78]. Reused and modified ACs have removal efficiencies below 40% that of the original [79]. Thus, it is imperative to seek another more efficient adsorbent to replace ACs. Based on the all aforementioned benefits and real samples investigations, PG-based materials are recommended for applications in wastewater treatment plants as a tertiary treatment option (such as filter media and continuous mixed systems) to remove ECs.

4. Conclusions

The growing use of pharmaceutical compounds and products classified as emerging contaminants (ECs) has recently raised considerable environmental concern worldwide. Driven by these environmental concerns, this study was aimed to evaluate the adsorption performance of porous graphene (PG), and compare it with other carbonaceous

materials (graphene oxide (GO) and graphite (GI)), as a potential candidate to remove a range of extensively used pharmaceuticals (atenolol (ATL), carbamazepine (CBZ), ciprofloxacin (CIP), diclofenac (DCF), gemfibrozil (GEM) and ibuprofen (IBP)) from water and wastewater. This study revealed i) fast adsorption kinetics of ECs onto PG guided by pseudo-second order model and adsorption capacities exceeding 100 mg-EC/g-PG for some of ECs; ii) high removal efficiencies for trace concentrations of all targeted ECs (> 99.9%) at a low dose of PG (100 mg/L); iii) multilayer and heterogeneous adsorption processes mainly followed the Toth and Sips adsorption isotherm models and controlled by physisorption mechanism, including electrostatic and π-π interactions, hydrogen bonding, and Van der Waals forces; iv) the robust adsorption performance of PG in real sample investigations, removing 99% of ECs in mixed solution systems at low dosages (250–500 mg/L); and v) the exothermic nature of the enthalpy-driven adsorption process (credited to negative values of the thermodynamic parameters), and confirmed the physical adsorption mechanism (ΔH values > -60 kJ/mol). Finally, PG had a good recyclability potential, which was demonstrated after its regeneration and reuse for four cycles in treating pharmaceutical-contaminated solutions. Further investigations are required to study the performance of these graphene-based materials as filter media for the removal of these ECs from surface waters and industrial wastewater samples.

Declaration of competing interests

The authors declare that they have no known competing financial interests or personal relationships that could have appeared to influence the work reported in this paper.

Acknowledgment

The presented research has been supported by the FAME (Fate and Management of Emerging Contaminants) Project, jointly funded by the Department of Science and Technology, Government of India (DST/TM/INDO-UK/2K17/66(C)) and the UK Natural Environment Research Council (NE/R003548/1) under India-UK Water Quality Programme. The research data supporting this publication are provided within this paper and as supplementary material.

Appendix A. Supplementary data

Supplementary data to this article can be found online at https://doi.org/10.1016/j.cej.2020.125440.

References

[1] M.J. Benotti, R.A. Trenholm, B.J. Vanderford, J.C. Holady, B.D. Stanford, S.A. Snyder, Pharmaceuticals and endocrine disrupting compounds in US drinking water, Environ. Sci. Technol. 43 (2008) 597–603.
[2] R. Baccar, M. Sarrà, J. Bouzid, M. Feki, P. Blánquez, Removal of pharmaceutical compounds by activated carbon prepared from agricultural by-product, Chem. Eng. J. 211–212 (2012) 310–317.
[3] C. Sophia, E.C. Lima, Removal of emerging contaminants from the environment by adsorption, Ecotoxicol. Environ. Saf. 150 (2018) 1–17.
[4] D.A. Lambropoulou, L.M. Nollet, Transformation Products of Emerging Contaminants in the Environment: Analysis, Processes, Occurrence, Effects and Risks, John Wiley & Sons, 2014.
[5] W.H. Organization, Pharmaceuticals in Drinking-Water, World Health Organization, 2012.
[6] S. Fekadu, E. Alemayehu, R. Dewil, B. Van der Bruggen, Pharmaceuticals in freshwater aquatic environments: a comparison of the African and European challenge, Sci. Total Environ. 654 (2019) 324–337.
[7] L. Rizzo, C. Manaia, C. Merlin, T. Schwartz, C. Dagot, M. Ploy, I. Michael, D. Fatta-Kassinos, Urban wastewater treatment plants as hotspots for antibiotic resistant bacteria and genes spread into the environment: a review, Sci. Total Environ. 447 (2013) 345–360.
[8] M. del Rosario Brunetto, S. Clavijo, Y. Delgado, W. Orozco, M. Gallignani, C. Ayala, V. Cerdà, Development of a MSFIA sample treatment system as front end of GC–MS for atenolol and propranolol determination in human plasma, Talanta 132 (2015) 15–22.
[9] A.A. Godoy, F. Kummrow, P.A.Z. Pamplin, Occurrence, ecotoxicological effects and risk assessment of antihypertensive pharmaceutical residues in the aquatic environment – a review, Chemosphere 138 (2015) 281–291.
[10] K.J. Meador, J. Seliger, A. Boyd, B. Razavi, J. Falco-Walter, S. Le, D.W. Loring, Comparative neuropsychological effects of carbamazepine and eslicarbazepine acetate, Epilepsy Behav. 94 (2019) 151–157.
[11] F. Pomati, S. Castiglioni, E. Zuccato, R. Fanelli, D. Vigetti, C. Rossetti, D. Calamari, Effects of a complex mixture of therapeutic drugs at environmental levels on human embryonic cells, Environ. Sci. Technol. 40 (2006) 2442–2447.
[12] M. Nkoom, G. Lu, J. Liu, H. Yang, H. Dong, Bioconcentration of the antiepileptic drug carbamazepine and its physiological and biochemical effects on Daphnia magna, Ecotoxicol. Environ. Saf. 172 (2019) 11–18.
[13] W.-T. Jiang, P.-H. Chang, Y.-S. Wang, Y. Tsai, J.-S. Jean, Z. Li, K. Krukowski, Removal of ciprofloxacin from water by birnessite, J. Hazard. Mater. 250 (2013) 362–369.
[14] C. Bouki, D. Venieri, E. Diamadopoulos, Detection and fate of antibiotic resistant bacteria in wastewater treatment plants: a review, Ecotoxicol. Environ. Saf. 91 (2013) 1–9.
[15] M. Schriks, M.B. Heringa, M.M.E. van der Kooi, P. de Voogt, A.P. van Wezel, Toxicological relevance of emerging contaminants for drinking water quality, Water Res. 44 (2010) 461–476.
[16] I.M. Sebastine, R.J. Wakeman, Consumption and environmental hazards of pharmaceutical substances in the UK, Process Saf. Environ. 81 (2003) 229–235.
[17] S.J. Khan, L. Wang, N.H. Hashim, J.A. Mcdonald, Distinct enantiomeric signals of ibuprofen and naproxen in treated wastewater and sewer overflow, Chirality 26 (2014) 739–746.
[18] P. Banerjee, P. Das, A. Zaman, P. Das, Application of graphene oxide nanoplatelets for adsorption of ibuprofen from aqueous solutions: evaluation of process kinetics and thermodynamics, Process Saf. Environ. 101 (2016) 45–53.
[19] S.T. Ulu, LC Determination of gemfibrozil in tablets, Chromatographia 64 (2006) 447–451.
[20] C. Mimeault, A.J. Woodhouse, X.S. Miao, C.D. Metcalfe, T.W. Moon, V.L. Trudeau, The human lipid regulator, gemfibrozil bioconcentrates and reduces testosterone in the goldfish, Carassius auratus, Aquat. Toxicol. 73 (2005) 44–54.
[21] A.C. Collier, Pharmaceutical contaminants in potable water: potential concerns for pregnant women and children, EcoHealth 4 (2007) 164–171.
[22] A. Jakimska, M. Śliwka-Kaszyńska, J. Reszczyńska, J. Namieśnik, A. Kot-Wasik, Elucidation of transformation pathway of ketoprofen, ibuprofen, and furosemide in surface water and their occurrence in the aqueous environment using UHPLC-QTOF-MS, Anal. Bioanal. Chem. 406 (2014) 3667–3680.
[23] D. Bendz, N.A. Paxéus, T.R. Ginn, F.J. Loge, Occurrence and fate of pharmaceutically active compounds in the environment, a case study: Höje River in Sweden, J. Hazard. Mater. 122 (2005) 195–204.
[24] H. Sanderson, D.J. Johnson, C.J. Wilson, R.A. Brain, K.R. Solomon, Probabilistic hazard assessment of environmentally occurring pharmaceuticals toxicity to fish, daphnids and algae by ECOSAR screening, Toxicol. Lett. 144 (2003) 383–395.
[25] K.S. Betts, Technology solutions: keeping drugs out of drinking water, Environ. Sci. Technol. 36 (2002) 377A–378A.
[26] S. Zhu, Y.-G. Liu, S.-B. Liu, G.-M. Zeng, L.-H. Jiang, X.-F. Tan, L. Zhou, W. Zeng, T.-T. Li, C.-P. Yang, Adsorption of emerging contaminant metformin using graphene oxide, Chemosphere 179 (2017) 20–28.
[27] A. Alazmi, O. El Tall, S. Rasul, M.N. Hedhili, S.P. Patole, P.M. Costa, A process to enhance the specific surface area and capacitance of hydrothermally reduced graphene oxide, Nanoscale 8 (2016) 17782–17787.
[28] Z. Pei, L. Li, L. Sun, S. Zhang, X.-Q. Shan, S. Yang, B. Wen, Adsorption characteristics of 1, 2, 4-trichlorobenzene, 2, 4, 6-trichlorophenol, 2-naphthol and naphthalene on graphene and graphene oxide, Carbon 51 (2013) 156–163.
[29] G.Z. Kyzas, E.A. Deliyanni, D.N. Bikiaris, A.C. Mitropoulos, Graphene composites as dye adsorbents: review, Chem. Eng. Res. Des. 129 (2018) 75–88.
[30] N. Baig, M. Ihsanullah, T.A. Sajid, Saleh, Graphene-based adsorbents for the removal of toxic organic pollutants: a review, J. Environ. Manage. 244 (2019) 370–382.
[31] G.Z. Kyzas, A. Koltsakidou, S.G. Nanaki, D.N. Bikiaris, D.A. Lambropoulou, Removal of beta-blockers from aqueous media by adsorption onto graphene oxide, Sci. Total Environ. 537 (2015) 411–420.
[32] S.-W. Nam, C. Jung, H. Li, M. Yu, J.R.V. Flora, L.K. Boateng, N. Her, K.-D. Zoh, Y. Yoon, Adsorption characteristics of diclofenac and sulfamethoxazole to graphene oxide in aqueous solution, Chemosphere 136 (2015) 20–26.
[33] H. Chen, B. Gao, H. Li, Removal of sulfamethoxazole and ciprofloxacin from aqueous solutions by graphene oxide, J. Hazard. Mater. 282 (2015) 201–207.
[34] N. Cai, P. Larese-Casanova, Sorption of carbamazepine by commercial graphene oxides: a comparative study with granular activated carbon and multiwalled carbon nanotubes, J. Colloid Interface Sci. 426 (2014) 152–161.
[35] Z. Niu, L. Liu, L. Zhang, X. Chen, Porous graphene materials for water remediation, Small 10 (2014) 3434–3441.
[36] T.A. Tabish, F.A. Memon, D.E. Gomez, D.W. Horsell, S. Zhang, A facile synthesis of porous graphene for efficient water and wastewater treatment, Sci. Rep. 8 (2018) 1817.
[37] L.L. Zhang, X. Zhao, M.D. Stoller, Y. Zhu, H. Ji, S. Murali, Y. Wu, S. Perales, B. Clevenger, R.S. Ruoff, Highly conductive and porous activated reduced graphene oxide films for high-power supercapacitors, Nano Lett. 12 (2012) 1806–1812.
[38] I. Jauris, C. Matos, C. Saucier, E. Lima, A. Zarbin, S. Fagan, F. Machado, I. Zanella, Adsorption of sodium diclofenac on graphene: a combined experimental and theoretical study, PCCP 18 (2016) 1526–1536.
[39] X. Zhu, D.C. Tsang, F. Chen, S. Li, X. Yang, Ciprofloxacin adsorption on graphene and granular activated carbon: kinetics, isotherms, and effects of solution

chemistry, Environ. Technol. 36 (2015) 3094–3102.
[40] T.P. Ferguson, J. Qu, The effect of moisture on the adhesion and fracture of interfaces in microelectronic packaging, in: E. Suhir, Y.C. Lee, C.P. Wong (Eds.) Micro- and Opto-Electronic Materials and Structures: Physics, Mechanics, Design, Reliability, Packaging, Springer US, Boston, MA, 2007, pp. B431-B471.
[41] K. Goebel, C.M.B. Rolim, Validation of UV spectrophotometric and HPLC methods for quantitative determination of atenolol in pharmaceutical preparations, Lat. Am. J. Pharm. 26 (2007) 765–770.
[42] N. Zadbuke, S. Shahi, A. Jadhav, S. Borde, Development and validation of uv-visible spectroscopic method for estimation of carbamazepine in bulk and tablet dosage form, Int. J. Pharm. Pharm. Sci. 8 (2016) 234–238.
[43] E.C.L. Cazedey, H.R.N. Salgado, Spectrophotometric determination of ciprofloxacin hydrochloride in ophthalmic solution, Adv. Anal. Chem. 2 (2012) 74–79.
[44] C. Parikh Vikas, V. Karkhanis, Spectrophotometric estimation of gemfibrozil in bulk and pharmaceutical dosage forms, Int. Res. J. Pharm. 2 (2011) 106–109.
[45] M.L. Farré, I. Ferrer, A. Ginebreda, M. Figueras, L. Olivella, L. Tirapu, M. Vilanova, D. Barceló, Determination of drugs in surface water and wastewater samples by liquid chromatography–mass spectrometry: methods and preliminary results including toxicity studies with Vibrio fischeri, J. Chromatogr. A 938 (2001) 187–197.
[46] S. Matongo, G. Birungi, B. Moodley, P. Ndungu, Pharmaceutical residues in water and sediment of Msunduzi River, kwazulu-natal, South Africa, Chemosphere 134 (2015) 133–140.
[47] N.K. Haro, P. Del Vecchio, N.R. Marcilio, L.A. Féris, Removal of atenolol by adsorption – study of kinetics and equilibrium, J. Cleaner Prod. 154 (2017) 214–219.
[48] I. Kong, Chapter 7 - Polymers with nano-encapsulated functional polymers, in: S. Thomas, R. Shanks, S. Chandrasekharakurup (Eds.), Design and Applications of Nanostructured Polymer Blends and Nanocomposite Systems, William Andrew Publishing, Boston, 2016, pp. 125–154.
[49] V. Kumar, K.-H. Kim, J.-W. Park, J. Hong, S. Kumar, Graphene and its nanocomposites as a platform for environmental applications, Chem. Eng. J. 315 (2017) 210–232.
[50] F. Mazloomi, M. Jalali, Ammonium removal from aqueous solutions by natural Iranian zeolite in the presence of organic acids, cations and anions, J. Environ. Chem. Eng. 4 (2016) 240–249.
[51] L.A. Al-Khateeb, S. Almotiry, M.A. Salam, Adsorption of pharmaceutical pollutants onto graphene nanoplatelets, Chem. Eng. J. 248 (2014) 191–199.
[52] A.M.E. Khalil, O. Eljamal, T.W.M. Amen, Y. Sugihara, N. Matsunaga, Optimized nano-scale zero-valent iron supported on treated activated carbon for enhanced nitrate and phosphate removal from water, Chem. Eng. J. 309 (2017) 349–365.
[53] M.R. Awual, T. Yaita, T. Taguchi, H. Shiwaku, S. Suzuki, Y. Okamoto, Selective cesium removal from radioactive liquid waste by crown ether immobilized new class conjugate adsorbent, J. Hazard. Mater. 278 (2014) 227–235.
[54] A. Shahat, H.M. Hassan, H.M. Azzazy, E. El-Sharkawy, H.M. Abdou, M.R. Awual, Novel hierarchical composite adsorbent for selective lead (II) ions capturing from wastewater samples, Chem. Eng. J. 332 (2018) 377–386.
[55] E. Alipanahpour Dil, M. Ghaedi, A. Asfaram, F. Mehrabi, A.A. Bazrafshan, Optimization of process parameters for determination of trace Hazardous dyes from industrial wastewaters based on nanostructures materials under ultrasound energy, Ultrason. Sonochem. 40 (2018) 238–248.
[56] H. Ji, H. Sun, X. Qu, Antibacterial applications of graphene-based nanomaterials: recent achievements and challenges, Adv. Drug Deliv. Rev. 105 (2016) 176–189.
[57] G. Bayramoglu, B. Altintas, M.Y. Arica, Adsorption kinetics and thermodynamic parameters of cationic dyes from aqueous solutions by using a new strong cation-exchange resin, Chem. Eng. J. 152 (2009) 339–346.
[58] A.C. Ferrari, Raman spectroscopy of graphene and graphite: Disorder, electron–phonon coupling, doping and nonadiabatic effects, Solid State Commun. 143 (2007) 47–57.
[59] T. Tabish, S. Chabi, M. Ali, Y. Xia, F. Jabeen, S. Zhang, Tracing the bioavailability of three-dimensional graphene foam in biological tissues, Materials 10 (2017) 336.
[60] L.M. Malard, M.A. Pimenta, G. Dresselhaus, M.S. Dresselhaus, Raman spectroscopy in graphene, Phys. Rep. 473 (2009) 51–87.
[61] A. Shahat, H.M. Hassan, H.M. Azzazy, M. Hosni, M.R. Awual, Novel nano-conjugate materials for effective arsenic (V) and phosphate capturing in aqueous media, Chem. Eng. J. 331 (2018) 54–63.
[62] M.R. Awual, M.M. Hasan, A.M. Asiri, M.M. Rahman, Cleaning the arsenic (V) contaminated water for safe-guarding the public health using novel composite material, Compos. Part B-Eng. 171 (2019) 294–301.
[63] T.A. Tabish, S. Zhang, P.G. Winyard, Developing the next generation of graphene-based platforms for cancer therapeutics: the potential role of reactive oxygen species, Redox Biol. 15 (2018) 34–40.
[64] T.A. Tabish, M.Z.I. Pranjol, D.W. Horsell, A.A. Rahat, J.L. Whatmore, P.G. Winyard, S. Zhang, Graphene oxide-based targeting of extracellular cathepsin D and cathepsin L as a novel anti-metastatic enzyme cancer therapy, Cancers 11 (2019) 319.
[65] T.A. Tabish, M.Z.I. Pranjol, H. Hayat, A.A. Rahat, T.M. Abdullah, J.L. Whatmore, S. Zhang, In vitro toxic effects of reduced graphene oxide nanosheets on lung cancer cells, Nanotechnology 28 (2017) 504001.
[66] T.A. Tabish, M.Z.I. Pranjol, F. Jabeen, T. Abdullah, A. Latif, A. Khalid, M. Ali, H. Hayat, P.G. Winyard, J.L. Whatmore, Investigation into the toxic effects of graphene nanopores on lung cancer cells and biological tissues, Appl. Mater. Today 12 (2018) 389–401.
[67] T.A. Tabish, C.J. Scotton, D.C.J. Ferguson, L. Lin, A.V. der Veen, S. Lowry, M. Ali, F. Jabeen, M. Ali, P.G. Winyard, Biocompatibility and toxicity of graphene quantum dots for potential application in photodynamic therapy, Nanomedicine 13 (2018) 1923–1937.
[68] B. Fadeel, C. Bussy, S. Merino, E. Vázquez, E. Flahaut, F. Mouchet, L. Evariste, L. Gauthier, A.J. Koivisto, U. Vogel, Safety assessment of graphene-based materials: focus on human health and the environment, ACS Nano 12 (2018) 10582–10620.
[69] T.A. Tabish, L. Lin, M. Ali, F. Jabeen, M. Ali, R. Iqbal, D.W. Horsell, P.G. Winyard, S. Zhang, Investigating the bioavailability of graphene quantum dots in lung tissues via Fourier transform infrared spectroscopy, Interface Focus 8 (2018) 20170054.
[70] L. Peng, Z. Xu, Z. Liu, Y. Wei, H. Sun, Z. Li, X. Zhao, C. Gao, An iron-based green approach to 1-h production of single-layer graphene oxide, Nat. Commun. 6 (2015) 5716.
[71] B. Kartick, S. Srivastava, Green synthesis of graphene, J. Nanosci. Nanotechnol. 13 (2013) 4320–4324.
[72] J. Bai, J. Chu, X. Yin, J. Wang, W. Tian, Q. Huang, Z. Jia, X. Wu, H. Guo, Z. Qin, Synthesis of amidoximated polyacrylonitrile nanoparticle/graphene composite hydrogel for selective uranium sorption from saline lake brine, Chem. Eng. J. 123553 (2019).
[73] A. Al Nafiey, A. Addad, B. Sieber, G. Chastanet, A. Barras, S. Szunerits, R. Boukherroub, Reduced graphene oxide decorated with Co_3O_4 nanoparticles (rGO-Co_3O_4) nanocomposite: a reusable catalyst for highly efficient reduction of 4-nitrophenol, and Cr(VI) and dye removal from aqueous solutions, Chem. Eng. J. 322 (2017) 375–384.
[74] T. Heberer, Tracking persistent pharmaceutical residues from municipal sewage to drinking water, J. Hydrol. 266 (2002) 175–189.
[75] S. Sadhukhan, S. Singha, U. Sarkar, Adsorption of para chloro meta xylenol (PCMX) in composite adsorbent beds: parameter estimation using nonlinear least square technique, Chem. Eng. J. 152 (2009) 361–366.
[76] M. Qurie, M. Khamis, F. Malek, S. Nir, S.A. Bufo, J. Abbadi, L. Scrano, R. Karaman, Stability and removal of naproxen and its metabolite by advanced membrane wastewater treatment plant and micelle–c lay complex, clean–soil, air, Water 42 (2014) 594–600.
[77] S.K. Behera, S.-Y. Oh, H.-S. Park, Sorption of triclosan onto activated carbon, kaolinite and montmorillonite: effects of pH, ionic strength, and humic acid, J. Hazard. Mater. 179 (2010) 684–691.
[78] P.K. Sharma, P.C. Wankat, Solvent recovery by steamless temperature swing carbon adsorption processes, Ind. Eng. Chem. Res. 49 (2010) 11602–11613.
[79] L. Wang, N. Balasubramanian, Electrochemical regeneration of granular activated carbon saturated with organic compounds, Chem. Eng. J. 155 (2009) 763–768.